JPL D-7194

SHUTTLE IMAGING RADAR-C GROUND DATA PROCESSING SYSTEM PROCESSING ALGORITHM DESIGN DOCUMENT

Version 1.2

C.Y. Chang

February 17, 1992

National Aeronautics and
Space Administration

JPL

Jet Propulsion Laboratory
California Institute of Technology
Pasadena, Ca 91109

SIR-C GDPS ALGORITHM DESIGN DOCUMENT

JPL D-7194

Prepared by:

C.Y. Chang
SIR-C GDPS Manager

Approved by:

John Curlander
SIR-C Ground Data System Manager

1. INTRODUCTION

The SIR-C processing algorithm design contains several unique characteristics as follows:

a) Large number of radar modes:

The SIR-C has two frequency bands, four polarization channels, up to twentythree data acquisition modes, two shuttle attitude modes, two range chirp bandwidths, three pulse durations, eight nominal PRFs, three input data sample quantizations, incidence angles from 15° up to 65°, and five types of data products. The processor must be capable and flexible to handle various radar modes and a large variation of processing parameters. The large number of radar modes complicates not only the software implementation but also the system integration and acceptance test.

b) Two processing modes: survey and standard:

The survey processor is a burst mode processor used for generation of quick-look imagery. The standard processor is a continuous mode processor used for generation of calibrated high resolution imagery. Both processors are distinct in algorithm design and require separate performance analysis.

c) High Doppler drift in both along-track and cross-track directions:

High Doppler drift requires frequent update of azimuth reference functions and range migration curves. Furthermore, the azimuth skew may be greater than a processing block, which is particularly true for the C-band case. The high Doppler drift also complicates the geometric rectification procedure to correctly assemble all the image blocks into a seamless strip image.

d) Multi-look filtering algorithm:

A new multi-look filtering algorithm is developed. The algorithm design is unique in the sense that with only small computation complexity permitted, it has to accomplish a number of functions altogether, such as resolution broadening control, sidelobe ratio control, speckle noise reduction and slant-to-ground range conversion.

e) Multi-frequency and multi-polarization data processing:

This requires proper generation of range and azimuth reference functions to ensure registration among multi-channel images and radiometric and phase calibration of data products.

1.1 Purpose

This document contains the processing algorithm design of the SIR-C Ground Data Processing System (GDPS). It covers detailed processing algorithm design and specifications required to process SAR signal data into desired image products. The purpose of this document is to demonstrate that this design can meet all the functional requirements set forth in the SIR-C GDPS Functional Requirements Document (JPL D-4892). This design document in conjunction with the Software Requirements Document and the Software Specifications Document will be used as the prime references to implement the SIR-C processor.

1.2 Scope

This document contains the processing algorithm design used to process SAR signal data into image products. Topics related to the data transfer, output product generation, radiometric and geometric calibration are not covered in this document.

The overall processing algorithms are organized into six different sets:

a) Initial processing parameters generation algorithm;

b) Turn-on and turn-off sequence processing algorithm;

c) Survey processing algorithm;

d) Standard preprocessing algorithm;

e) Standard processing algorithm;

f) Standard postprocessing algorithm; and

g) Quality assurance algorithm.

The initial processing parameters generation algorithm contains a number of routines used [o derive the initial Doppler predicts from the ephemeris parameters, the image geodetic locations and other processing and image related parameters. The turn-on and turn-off sequence processing algorithm is designed to process the receive only noise data, caltone scan data and PRF scan data. The survey processing algorithm is employed to process the entire data of a data take into survey image products. The standard preprocessing algorithm is employed to refine the Doppler centroid and Doppler frequency rate estimates. The standard processing algorithm is employed to process a segment of data into standard image products. The quality assurance algorithm is employed to assure the data quality at each processing stage.

1.3 Table of Contents

1.4 List of Tables and Figures

List of Tables

List of Figures

1.5 Applicable Documents

JPL Documents:

1. SIR-C Functional Requirement Document, JPL D-2826, (updated), May 1991.
2. SIR-C GDPS Functional Requirements Document, JPL D-4892, (updated), January, 1992.
3. SIR-C GDPS Functional Desire Document, JPL D-4983, April 1989.
4. SIR-C Calibration Processor System Functional Design Document, JPL D-6953, January 1990.
5. Data Products and Image Quality Specifications for the SIR-C/X-SAR Mission, JPL D-7193, (updated), January 1991.
6. SIR-C GDPS Software Requirements Document, JPL D-641O, (updated), October 1990.
7. SIR-C GDPS Software Specifications Document, JPL D-8418, February 1992.
8. SIR-C GDPS Acceptance Test Plan Document, JPL D-8417, June 1991.

Technical Papers:

9. F. Li, et al, "Doppler Centroid Estimation for Spaceborne Synthetic Aperture Radars, " IEEE Trans. on Geoscience and Remote Sensing, Vol. GE-23, No. 1, pp. 47-56, Jan 1985.
10. F. Li, et al, "Comparison of Several Techniques to Obtain Multiple-Look SAR Imagery, " IEEE Trans. on Geoscience and Remote Sensing, Vol. GE-21, No. 3, pp. 370-375, July, 1983.
11. M. Jin, et al, "A SAR Correlation Algorithm which Accommodates Large Range Migration, " IEEE Trans. on Geoscience and Remote Sensing, Vol. GE-22, No. 6, pp. 592-597, Nov, 1984.
12. J. van Zyl, et al, "Data Volume Reduction for Single-L.ook Polarimetric Imaging Radar Data, " submitted to IEEE Trans. on Geoscience and Remote Sensing.

JPL Interoffice Memos:

13. K. Leung, "Weighting Effects on Point Target Response, " JPL IOM 3344-82-039, Sept 20, 1982.
14. R. Carande, "SPS Preprocessing: Initial Doppler Parameter Calculation, " JPL IOM 3347-88-002, March 30, 1988,
15. P. Dubois, "Note on the Compression Algorithm, " JPL IOM 3348-88-70, July 14, 1988.
16. R. Carande, "SPS Geolocation Algorithm and Verification, " JPL IOM 3347-88-017, Aug 10, 1988.
17. R. Carande, "Slant Range to Ground Range Conversion for the ASP, " JPL IOM 3347-88-023, Sept 30, 1988.

18. R. Carande, "Calculating Range Radiometric Correction Vector, " JPL 3347-89-002, Jan 19, 1989.

19, C.Y. Chang and S.S. Pang, "SIR-C Survey Processing Algorithm, " JPL 3348-89-030, March 17, 1989.

20. K. Leung, " Registration of H & V Transmitted Data for SIR-C, " JPL 3348-89-032, March 21, 1989.

21. C.Y. Chang, "Simulated Point Target Data Generation Algorithm," JPL IOM 3348-89-068, June 8, 1989.

22. C.Y. Chang, "Azimuth Deskew Algorithm Considering Along-Track Doppler Update", JPL 10M 3348-89-064, June 8, 1989.

23. C.Y. Chang, "Standard Processing Algorithm Complexity Analysis," JPL IOM **3348-89-072,** June 9, 1989.

24. C.Y. Chang, "SIR-C Standard Processing Algorithm, " JPL IOM 3348-89-073, June 21, 1989.

25. C.Y. Chang, "SIR-C Standard Preprocessing Algorithm Complexity Analysis," JPL IOM 3348-89-077, June 22, 1989.

26. C.Y. Chang, "Geometric Calibration," JPL IOM 3348-89-060, Aug 10, 1989,

27. J. C-. Curlander and C.Y. Chang, "Selection of Processing Bandwidth for the SIR-C Processor," JPL IOM 3348-89-108, Aug 11, 1989.

28. C.Y. Chang, "Survey Processing Algorithm Complexity Analysis," JPL IOM 3348-89-112, Aug 23, 1989.

29. C.Y. Chang and S.S, Pang, "Survey Processor Test Results," JPL IOM 3348-89-113, Aug 30, 1989.

30. C.Y. Chang and S.S. Pang, "Ambiguity-to-Signal Ratio, Signal Loss and Scalloping," JPL IOM 3348-89-114, Aug 30, 1989.

31. C.Y. Chang, "Radar System and Processing Parameter Analysis," JPL IOM 3348-89-115, Sept 14, 1989.

32. D.D. Perz, "SIR-C Processor Throughput Analysis, " JPL IOM 3348-89-117, Sept 20, 1989.

33. C.Y. Chang, "Memory Configuration Design Trade-Off, " JPL IOM 3348-89-122, Sept 20, 1989.

34. C.Y. Chang, "Data Q/A Algorithm, " JPL IOM 3348-89-140, Ott 5, 1989.

35, C.Y. Chang and S.S. Pang, "Sensor Position Measurement Refinement, " JPL IOM 3348-89-128, Ott 10, 1989.

36. K. Vines, "SIR-C Q/A Processing Parameters Definition and Operation, " JPL IOM 3348-89-151, Ott 19, 1989,

37. C.Y. Chang and S.S. Pang, "Autofocus and Clutterlock Study, " JPL IOM 3348-89-165, Nov 9, 1989.

38. J.C. Curlander, "Summary of SIR-C Processor Requirements Meeting, " JPL IOM 3348-89-166, Nov 16, 1989.

39. C.Y. Chang, "SIR-C Survey and Standard Processing Operational Scenario, " JPL IOM 3348-89-140, Nov 27, 1989.

40. C.Y. Chang and S.S. Pang, "Survey Doppler Frequency Rate Estimation, " JPL 10M 3348-89-141, Nov 27, 1989.

41. C.Y. Chang, "Point-Target Response Performance Measurement, " JPL IOM 3348-89-180, Nov 28, 1989,

42. K. Vines, "SIR-C Q/A Parameter File Definition, " JPL IOM 3348-89-181, Dec 11, 1989.

43. J.C. Curlander, C.Y. Chang, D.D. Perz, "SIR-C Survey and Standard Data Segment Length Analysis Results, " JPL IOM 3348-89-184, Dec 12, 1989.

44. J.C. Curlander and C.Y. Chang, "Summary of the Second SIR-C Processor Requirement Meeting, " JPL IOM 3348-89-192, Dec 28, 1989.

45. J.C. Curlander and C.Y. Chang, "SIR-C Standard Data Product Specification Update, " JPL IOM 3348-89-192, Dec 28, 1989.

46. C.Y. Chang and S.S. Pang, "Multi-Look Processing Algorithm, " JPL IOM 3348-90-002, Jan 8, 1990.

47. C.Y. Chang, "SIR-C Initial Processing Parameter Determination Algorithm, " JPL IOM 3348-90-008, Jan 11, 1990.

48. P. Dubois and J. van Zyl, "Cress-Product Compression, " JPL IOM 3348-89-195, Jan 30, 1990.

49. J.C. Curlander and C.Y. Chang, "Effects of Jitter Error, Electronic Delay Error and STALO Drift Error on Image Quality and Their Specifications, " JPL IOM 3348-90-060, April 16, 1990.

50. C.Y. Chang, "Turn-On and Turn-Off Sequence Processing, " JPL IOM 3348-090-088, June 8, 1990.

51. C.Y. Chang, "Swath Truncation, " JPL IOM 3348-90-094, June 15, 1990.

52. C.Y. Chang, "Standard Processing Algorithm Complexity Analysis Update, " JPL IOM 3348-90-095, Sept 171990,

53. C.Y. Chang, "SIR-C PRF Selection Procedure (Revised), " JPL IOM 3348-90-089, Ott 31990.

54. C.Y. Chang and S.S. Pang, "Sidelobe Analysis of Multi-Look Processing Algorithm, " JPL IOM 3348-90-124, Ott 12, 1990.

55. C.Y. Chang and S.S. Pang, "Analysis of Residual Range Migration Error Effects (Updated), " IOM 3348-90-123, Ott.22, 1990.

56. C.Y. Chang, "Yaw Steering to Zero-Doppler Line for SIR-C, " JPL IOM 3348-90-133, Ott 26, 1990.

57. C.Y. Chang, "Standard Azimuth Compression Algorithm, " JPL IOM 3348-90-134, Nov 5, 1990.

58, C.Y. Chang, "SIR-C Survey Processor Geometric Rectification Algorithm, " JPL IOM 3348-90-135, Dec 12, 1990.

59. C.Y. Chang, "A Few Notes on the Near Range Slant Range, " JPL IOM 3348-91-000, Feb 4, 1990.

60. C.Y. Chang, "Some Thoughts on Doppler Parameter Analysis, " JPL IOM 3348-91-000, Feb 18, 1991.

61. C.Y. Chang, "Advantages of Yaw Steering Technique, " JPL IOM 3348-91-000, . Feb 18, 1991.

62. C.Y. Chang, "Selection of Scale Factor in Data Packing, " JPL IOM 3348-91-000, March 1, 1991.

63. C.Y. Chang, "Standard Processing Algorithm Complexity Analysis Update, " JPL IOM 3348-91-000, March 12, 1991.

64. C.Y. Chang, "Standard Preprocessing Algorithm Complexity Analysis Update, " JPL 10M 3348-91-000, March 12, 1991.

65. C.Y. Chang, "Survey Processing Algorithm Complexity Analysis Update, " JPL IOM 3348-91-000, March 12, 1991.

66. C.Y. Chang, "Requirements on Antenna Pattern Generation Software, " JPL IOM 3348-91-048, Aug 7, 1991.

67. C.Y. Chang, "L-Band and C-Band Image Registration, " JPL IOM 3348-91-049, Aug 19, 1991.

68. C.Y. Chang, "Telemetry Processing Scenario for Antenna Pattern Generation, " JPL IOM 3348-91-052, Aug 20, 1991.

69. C.Y. Chang, "Survey Processor Geometric Rectification Algorithm, " JPL IOM 3348-91-000, September 26, 1991.

70. C.Y. Chang, "Attitude Steering to Zero-Doppler Technique, " JPL IOM 3348-91-001, Jan 10, 1992.

1.5 Applicable Documents

JPL Documents:

1. SIR-C Functional Requirement Document, JPL D-2826, (updated), May 1991.
2. SIR-C GDPS Functional Requirements Document, JPL D-4892, (updated), January, 1992.
3. SIR-C GDPS Functional Design Document, JPL D-4983, April 1989.
4. SIR-C Calibration Processor System Functional Design Document, JPL D-6953, January 1990.
5. Data Products and Image Quality Specifications for the SIR-C/X-SAR Mission, JPL D-7193, (updated), January 1991.
6. SIR-C GDPS Software Requirements Document, JPL D-641O, (updated), October 1990.
7. SIR-C GDPS Software Specifications Document, JPL D-8418, February 1992.
8. SIR-C GDPS Acceptance Test Plan Document, JPL D-8417, June 1991.

Technical Papers:

9. F. Li, et al, "Doppler Centroid Estimation for Spaceborne Synthetic Aperture Radars, " IEEE Trans. on Geoscience and Remote Sensing, Vol. GE-23, No. 1, pp. 47-56, Jan 1985.
10. F. Li, et al, "Comparison of Several Techniques to Obtain Multiple-Look SAR Imagery, " IEEE Trans. on Geoscience and Remote Sensing, Vol. GE-21, No. 3, pp. 370-375, July, 1983.
11. M, Jin, et al, "A SAR Correlation Algorithm which Accommodates Large. Range Migration, " IEEE Trans. on Geoscience and Remote Sensing, Vol. GE-22, No. 6, pp. 592-597, Nov, 1984.
12. J. van Zyl, et al, "Data Volume Reduction for Single-Look Polarimetric Imaging Radar Data, " submitted to IEEE Trans. on Geoscience and Remote Sensing.

JPL Interoffice Memos:

13. K. Leung, "Weighting Effects on Point Target Response, " JPL IOM 3344-82-039, Sept 20, 1982.
14. R. Carande, "SPS Preprocessing: Initial Doppler Parameter Calculation, " JPL IOM 3347-88-002, March 30, 1988.
15. P. Dubois, "Note on the Compression Algorithm, " JPL IOM 3348-88-70, July 14, 1988.
16. R. Carande, "SPS Geolocation Algorithm and Verification, " JPL IOM 3347-88-017, Aug 10, 1988,
17. R. Carande, "Slant Range to Ground Range Conversion for the ASP, " JPL IOM 3347-88-023, Sept 30, 1988.

18. R. Carande, "Calculating Range Radiometric Correction Vector, " JPL 3347-89-002, Jan 19, 1989.

19. C.Y. Chang and S.S. Pang, "SIR-C Survey Processing Algorithm, " JPL 3348-89-030, March 17, 1989.

20. K. Leung, " Registration of H & V Transmitted Data for SIR-C, " JPL 3348-89- , 032, March 21, 1989.

21. C.Y. Chang, "Simulated Point Target Data Generation Algorithm," JPL IOM 3348-89-068, June. 8, 1989.

22. C.Y. Chang, "Azimuth Deskew Algorithm Considering Along-Track Doppler Update", JPL IOM 3348-89-064, June 8, 1989.

23. C.Y. Chang, "Standard Processing Algorithm Complexity Analysis," JPL IOM 3348-89-072, June 9, 1989.

24. C.Y. Chang, "SIR-C Standard Processing Algorithm, " JPL IOM 3348-89-073, June 21, 1989.

25. C.Y. Chang, "SIR-C Standard Preprocessing Algorithm Complexity Analysis," JPL IOM 3348-89-077, June 22, 1989.

26. C.Y. Chang, "Geometric Calibration," JPL IOM 3348-89-060, Aug 10, 1989,

27. J.C. Curlander and C.Y. Chang, "Selection of Processing Bandwidth for the SIR-C Processor," JPL 10M 3348-89-108, Aug 11, 1989.

28. C.Y. Chang, "Survey Processing Algorithm Complexity Analysis," JPL IOM 3348-89-112, Aug 23, 1989.

29. C.Y. Chang and S.S. Pang, "Survey Processor Test Results," JPL IOM 3348-89-113, Aug 30, 1989.

30. C.Y. Chang and S.S. Pang, "Ambiguity-to-Signal Ratio, Signal Loss and Scalloping," JPL IOM 3348-89-114, Aug 30, 1989.

31. C.Y. Chang, "Radar System and Processing Parameter Analysis," JPL IOM 3348-89-115, Sept 14, 1989.

32. D.D. Perz, "SIR-C Processor Throughput Analysis, " JPL IOM 3348-89-117, Sept 20, 1989.

33. C.Y. Chang, "Memory Configuration Design Trade-Off, " JPL IOM 3348-89-122, Sept 20, 1989.

34. C.Y. Chang, "Data Q/A Algorithm, " JPL IOM 3348-89-140, Oct 5, 1989.

35. C.Y. Chang and S.S. Pang, "Sensor Position Measurement Refinement, " JPL 10M 3348-89-128, Ott 10, 1989.

36. K. Vines, "SIR-C Q/A Processing Parameters Definition and Operation, " JPL IOM 3348-89-151, Ott 19, 1989.

37. C.Y. Chang and S.S, Pang, "Autofocus and Clutterlock Study, " JPL IOM 3348-89-165, Nov 9, 1989.

38. J.C. Curlander, "Summary of SIR-C Processor Requirements Meeting, " JPL IOM 3348-89-166, Nov 16, 1989.

39. C.Y. Chang, "SIR-C Survey and Standard Processing Operational Scenario, " JPL IOM 3348-89-140, Nov 27, 1989.

40. C.Y. Chang and S.S. Pang, "Survey Doppler Frequency Rate Estimation, " JPL IOM 3348-89-141, Nov 27, 1989.

41. C.Y. Chang, -"Point-Target Response Performance Measurement, " JPL 10M 3348-89-180, Nov 28, 1989.

42. K. Vines, "SIR-C Q/A Parameter File Definition, " JPL IOM 3348-89-181, Dec 11, 1989.

43. J.C. Curlander, C.Y. Chang, D.D. Perz, "SIR-C Survey and Standard Data Segment Length Analysis Results, " JPL IOM 3348-89-184, Dec 12, 1989.

44. J.C. Curlander and C.Y. Chang, "Summary of the Second SIR-C Processor Requirement Meeting, " JPL IOM 3348-89-192, Dec 28, 1989.

45. J.C. Curlander and C.Y. Chang, "SIR-C Standard Data Product Specification Update, " JPL IOM 3348-89-192, Dec 28, 1989.

46. C.Y. Chang and S.S. Pang, "Multi-Look Processing Algorithm, " JPL IOM 3348-90-002, Jan 8, 1990.

47. C.Y. Chang, "SIR-C Initial Processing Parameter Determination Algorithm, " JPL IOM 3348-90-008, Jan 11, 1990.

48. P. Dubois and J. van Zyl, "Cross-Product Compression, " JPL IOM 3348=89- 195, Jan 30, 1990.

49. J.C. Curlander and C.Y. Chang, "Effects of Jitter Error, Electronic Delay Error and STALO Drift Error on Image Quality and Their Specifications, " JPL IOM 3348-90-060, April 16, 1990.

50. C.Y. Chang, "Turn-On and Turn-Off Sequence Processing, " JPL 10M 3348-090-088, June 8, 1990.

51. C.Y. Chang, "Swath Truncation, " JPL IOM 3348-90-094, June 15, 1990.

52. C.Y. Chang, "Standard Processing Algorithm Complexity Analysis Update, " JPL IOM 3348-90-095, Sept 171990.

53. C.Y. Chang, "SIR-C PRF Selection procedure (Revised), " JPL IOM 3348-90-089, Ott 31990.

54. C.Y. Chang and S.S. Pang, "Sidelobe Analysis of Multi-Look Processing Algorithm, " JPL IOM 3348-90-124, Oct 12, 1990.

55. C.Y. Chang and S.S, Pang, "Analysis of Residual Range Migration Error Effects (Updated), " IOM 3348-90-123, Ott 22, 1990,

56. C.Y. Chang, "Yaw Steering to Zero-Doppler Line for SIR-C, " JPL IOM 3348-90-133, Ott 26, 1990.

57. C.Y. Chang, "Standard Azimuth Compression Algorithm, " JPL IOM 3348-90-134, Nov 5, 1990.

58. C.Y. Chang, "SIR-C Survey Processor Geometric Rectification Algorithm, " JPL IOM 3348-90-135, Dec 12, 1990.

59. C.Y. Chang, "A Few Notes on the Near Range Slant Range, " JPL IOM 3348-91-000, Feb 4, 1990.

60. C.Y. Chang, "Some Thoughts on Doppler Parameter Analysis, " JPL IOM 3348-91-000, Feb 18, 1991.

61. C.Y. Chang, "Advantages of Yaw Steering Technique, " JPL IOM 3.348-91-000, Feb 18, 1991.

62. C.Y. Chang, "Selection of Scale Factor in Data Packing, " JPL IOM 3348-91-000, March 1, 1991.

63. C.Y. Chang, "Standard Processing Algorithm Complexity Analysis Update, " JPL IOM 3348-91-000, March 12, 1991.

64. C.Y. Chang, "Standard Preprocessing Algorithm Complexity Analysis Update, " JPL IOM 3348-91-000, March 12, 1991.

65. C.Y. Chang, "Survey Processing Algorithm Complexity Analysis Update, " JPL 10M 3348-91-000, March 12, 1991,

66. C.Y. Chang, "Requirements on Antenna Pattern Generation Software, " JPL IOM 3348-91-048, Aug 7, 1991.

67. C.Y. Chang, "L-Band and C-Band Image Registration, " JPL IOM 3348-91-049, Aug 19, 1991.

68. C.Y. Chang, "Telemetry Processing Scenario for Antenna Pattern Generation, " JPL IOM 3348-91-052, Aug 20, 1991.

69. C.Y. Chang, "Survey Processor Geometric Rectification Algorithm, " JPL IOM 3348-91-O(X), September 26, 1991.

70. C.Y. Chang, "Attitude Steering to Zero-Doppler Technique, " JPL IOM 3348-91-001, Jan 10, 1992.

2. SYSTEM REQUIREMENTS

This section documents system requirements of the SIR-C Ground Data Processing System (GDPS). These system requirements are divided into the following four categories: a) Orbit characteristics: b) Radar system characteristics; c) Processor image quality requirements: and d) Processing parameter requirements.

2.1 Orbit Characteristics

The SIR-C radar is flown on the NASA Space. Transportation System (Shuttle) with the following orbital and attitude characteristics:

1: Orbital Characteristics:

a) Nominal Altitude: 215 km ± 25 km,

b) Eccentricity: <0.002

c) Inclination: 57°

2. Position Error (3u):

a) along-track: ±3.048 Km

b) cross-track: ±0.610 Km

c) radial: ±0.549 Km

3. Velocity Error (3σ):

a) along-track: ±0.549 m/sec

b) cross-track: 40.S8L1 m/sec

c) radial: ±3.353 m/see

4. Attitude Error:

Measurement (3σ):

a) roll: ±1.24°

b) yaw: ±1.43°

c) pitch: ±1.78°

Drift Rate (3σ):

a) roll: ±0.03°/sec

b) yaw: ±0.03 °/see

c) pitch: ±0.03°/sec

2.2 Radar System Characteristics

The characteristics of the SIR-C synthetic aperture radar are listed as follows:

1. Radar Transmit. Center Frequency:

   a) L-Band (20 MHz Bandwidth): 1248.6261 ±0.1 MHz

   b) 1,-Band (10 MHz Bandwidth): 1254.2947± 0.1 MHz

   c) C-Band (20 MHz Bandwidth): 5298.3669±0.1 MHz

   d) C-Band (10 MHz Bandwidth): .5304,03 56±0.1 MHz

2. Polarization:

   a) Simultaneous HH, HV, VH, VV

   b) Cross Polarization Isolation: ≥ 20 dB

3. Antenna Boresight Alignment (1σ):

   a) LH to LV: ≤ 0.020° in azimuth, ≤ O.1° in elevation

   b) CH to CV: <0.005° in azimuth, ≤ 0.1° in elevation

4. Incidence Angle: 17° - 63°, maximum incidence angle for the quad-polarization mode: 45°

5. Swath Width:

   a) Minimum Ground Swath: 15 Km

   b) Maximum Ground Swath: 90 Km

6. Noise Equivalent σ_0:

   a) L-Band: -40 dB at 50°

   b) C-Band: -36 dB at 50°

i. Range Chirp:

   a) Slope: linear FM down chirp

   b) Bandwidth: 10±0.01 MHz, 203-0.01 MHz

   c) Pulse Duration: 33.8/16.9/8.44±0.01 micro-second

   d) Real Sampling Rate: ?2.5 MHz (STALO/4), 45.0 MHz (STALO/2)

8. Data Sample Format: 4 bit, 8 bit or (8,4) BFPQ

9. Electronic Timing Error (1σ):

   a) Absolute A/Ii Jitter Error: 50 pico-second

   b) Relative A/D Jitter Error: 1 nano-second

   c) Absolute Electronic Delay Time Error: 25 nano-second

   d) Relative Electronic Delay Time Error: 5 nano-second

10. Data Rate: 45 M bits/see x 4 channels

11. Data Source: HDDT (Cassettes)

12. Data Volume: 50 hrs x 4 channels

13. Pulse Repetition Frequencies: 16 values

    Nominal : (1344.0Hz 1395.0Hz 1440.0112 1488.0Hz
    1512.0Hz 1620.0Hz 1674.0Hz 1736.0Hz)

    Anomalous : 1240.0Hz 1260.0Hz 1302.0Hz 1860.0Hz
    (1S90.0112 1953,0112 2016.0Hz 2160.0Hz)

14. STALO Frequency:

    a) STALO Frequency: 89.994240 MHz ± TBD Hz

    b) STALO Drift Rate: $\leq$ 2 parts per million per year

    c) STALO Drift Uncertainty: $\leq$ 20%

15. Data Window Position Interval: 4.9780964- micro-second (or 448/STALO)

16. Antenna:

    a) Physical Size: 12.1 m x 2,80 m for L-[land, 12.1 m x 0.74 m for C-Band, (12.1 m x 0.40 m for X-SAR)

    b) Radiated Power: 4.317 KW for L-Band. 2.285 KW for C-Band

17. Dynamic Range:

    a) Distributed Targets: 20 dB

    b) Point Targets: 40 dB

18. One-Dimensional Impulse Response ISLR: - 12 dB overall, –14 dB processor

2.3 Processor image Quality Requirements

All the standard image data products shall meet or exceed the following specifications:

1. Spatial Resolution Broadening:
   a) Range: $\leq 20\%$
   b) Azimuth: $\leq$ 20%
2. PSLR:
   a) Range: ≤ -17 dB
   b) Azimuth: ≤ -17 dB
3. ISLR:
   a) Range: ≤ -14 dB
   b) Azimuth: ≤ -14 dB
4. Azimuth Ambiguity to Signal Ratio (ASR): ≤ -20 dB
5. Swath Width:
   a) Minimum Ground Swath: 15 Km
   b) Maximum Ground Swath: 90 Km
6. Radiometric Accuracy (Science Goal):
   a) Relative Cross-Swath (1σ): ± 0.2 dB
   b) Relative Band-to-Band (1σ): ± 1.5 dB
   c) Relative Channel-to-Channel (1σ): ± 1.0 dB
   d) Absolute Each Channel (3σ): ± 3.0 dB
7. Geometric Accuracy (3σ):
   a) Absolute Location: ≤ 100 m
   b) Registration:
      Pol-to-pol: $\leq$ 1/8 pixel
      Band-to-band: $\leq$ 1/8 pixel
   c) Geometric Rectification:
      Scale: $\leq$ 0.1%
      Skew: $\leq$ 0.1%

2.4 Processing Parameter Requirements

'l'his section summarizes processing parameter analysis results based on the given orbit and radar system characteristics.

2.4.1 Doppler Bounds

'Table 2.1 shows the Doppler bounds of the SIR-C I,- band, C-band and the X-SAR at 57° inclination angle.

2.4.2 Doppler Drift Rates

Table 2.2 shows the worst case along-track and cross-track Doppler drift rates of the SIR-C 1,-band, C-band and the X-SAR at 57° inclination angle.

2.4.3 Doppler Update Rate

Table 2.3 shows the worst case along-track and cross-track Doppler update rates of the SIR-C L-band, C-band and the X-SAR at 57° inclination angle. The update criteria are

a) 10% PBW for the Doppler centroid;

b) 1 /7"^{2}(π/4 quadratic phase error) for the Doppler frequency rate, where T represents the full synthetic aperture time.

2.4.4 Range Migration Extent

Table 2.4 shows the maximum range walk and range curvature of the SIR-C L-band. C-band and the X-SAR at 57° inclination angle for high resolution mode (20 MHz range chirp bandwidth) and low resolution mode (10 MHz range chirp bandwidth).

2.4.5 Synthetic Aperture Time

Table 2.5 shows the synthetic aperture time and length of the SIR-C L-band, C-band and the X-SAR at 57° inclination angle.

Doppler Bound	SIR-C L-BAND	SIR-C C-BAND	X-SAR
F_d (Hz) [1]	± 5300	± 22000	± 39800
F_r (Hz/sec) [2]	2100, 800	8700 , 3400	15800, 6100

Table 2.1: Doppler Bounds for the SIR-C L-band, C-band and the X-SAR at 57" inclination angle.
[1]: High look angle.
[2]: Low, anti high look angles,

Doppler Drift Rate	SIR-C L-BAND	SIR-C C-BAND	X-SAR
ALONG-TRACK			
f_d (Hz/sec) [3]	57	236	428
F_r (Hz/sec^2) [2]	0.03, 0.01	0.12, 0.04	0.23, 0,08
CROSS-TRACK			
F_d (Hz/Km) [2]	78, 3	325, 13	587, 23
F_r (Hz/sec/Km) [2]	6.7, 1.1	27.9, 4.6	50,4, 8.3

Table 2.2: Worst case Doppler drift rate for the SIR-C L-band, C-band and the X-SAR at 57° inclination angle,
[1]: High look angle.
[2]: Low, and high look angles.
[3]: 45° look angle.

Doppler Update Rate	SIR-C L-BAND	SIR-C C-BAND	X-SAR
ALONG-TRACK			
F_d (see) [3]	2.63	0.63	0.35
F_r ($s_{e\,c}$) [2]	43, 21	181, 87	326, 156
CROSS-TRACK			
'd (m) [2]	641, 16667	154, 4007	85, 2216
F_r (m) [2]	194, 189	807, 786	1459, 1421

Table 2.3: Worst case Doppler update rate for the SIR-C L-band, C-band and the X-SAR at 57° inclination angle,

[1]: High look angle,

[2]: Low, and high look angles.

[3]: 45° look angle.

[4]: fd error budget: along-track: 6% DBW; cross-track 2% DBW; clutterlock: 2% DBW.

[5]: fr (quadratic phase) error budget: along-track: n/16; cross-track: π/16; autofocus: π/8.

RANGE WALK/CURVATURE (BINs)	SIR-C L-BAND	SIR-C C-BAND	X-SAR
10 MHz (13.4 m)	72/2.1	17/0.12	10/0.04
20 MHz (6.7 m)	144/4.3	35/0.25	19/0.08

Table 2.4: Maximum range walk/range curvature for the SIR-C L-band, C-band and the X-SAR at 57° inclination angle.

	SIR-C L-BAND	SIR-C C-BAND	X-SAR
TIME (see)	0.425 - 1.545	0.102 - 0.371	0.057 - 0.205
LENGTH (pulses)	571 - 2638	137 - 645	76 - 357

Table 2.5: Synthetic aperture time and length for the SIR-C L-band, C-band and the X-SAR at 57° inclination angle.

3. DATA CHARACTERISTICS

This section defines the SIR-C GDPS nput data run format and output da a product format.

3.1 Input Data Run Format

The data format of a SIR-C nominal recorded data acquisition sequence is shown in Fig. 3.1. It is composed of three data sequences: a) Turn-on sequence; b) Data take sequence: and c) Turn-off sequence. Each segment in turn-on and turn-off sequence is one second duration,

There are two types of turn-on sequence format: BITE and no BITE. The BITE format consists of the following data segments for a total of six seconds.

a) One second Receive Only Seise data:

b) One second Caltone Scan data;

c) One second LNA data;

d) One second HPA data;

e) One second PRF_A data;

f) One second PRF_B data.

The no BITE format consists of the following data segments for a total of six seconds.

a) Four second Receive Only Noise data;

b) One second PRF_A data;

c) One second PRF_B data.

The data take sequence contains the raw signal data acquired using PRF_C for an average duration of 8.5 minutes.

The turn-off sequence data consists of the following data segments for a total of six seconds.

a) One second PRF_B data;

b) One second PRF_A data;

c) Four second Receive Only Noise data.

The null-line data used for estimation of the shuttle roll angles are inserted at every second time ticks.

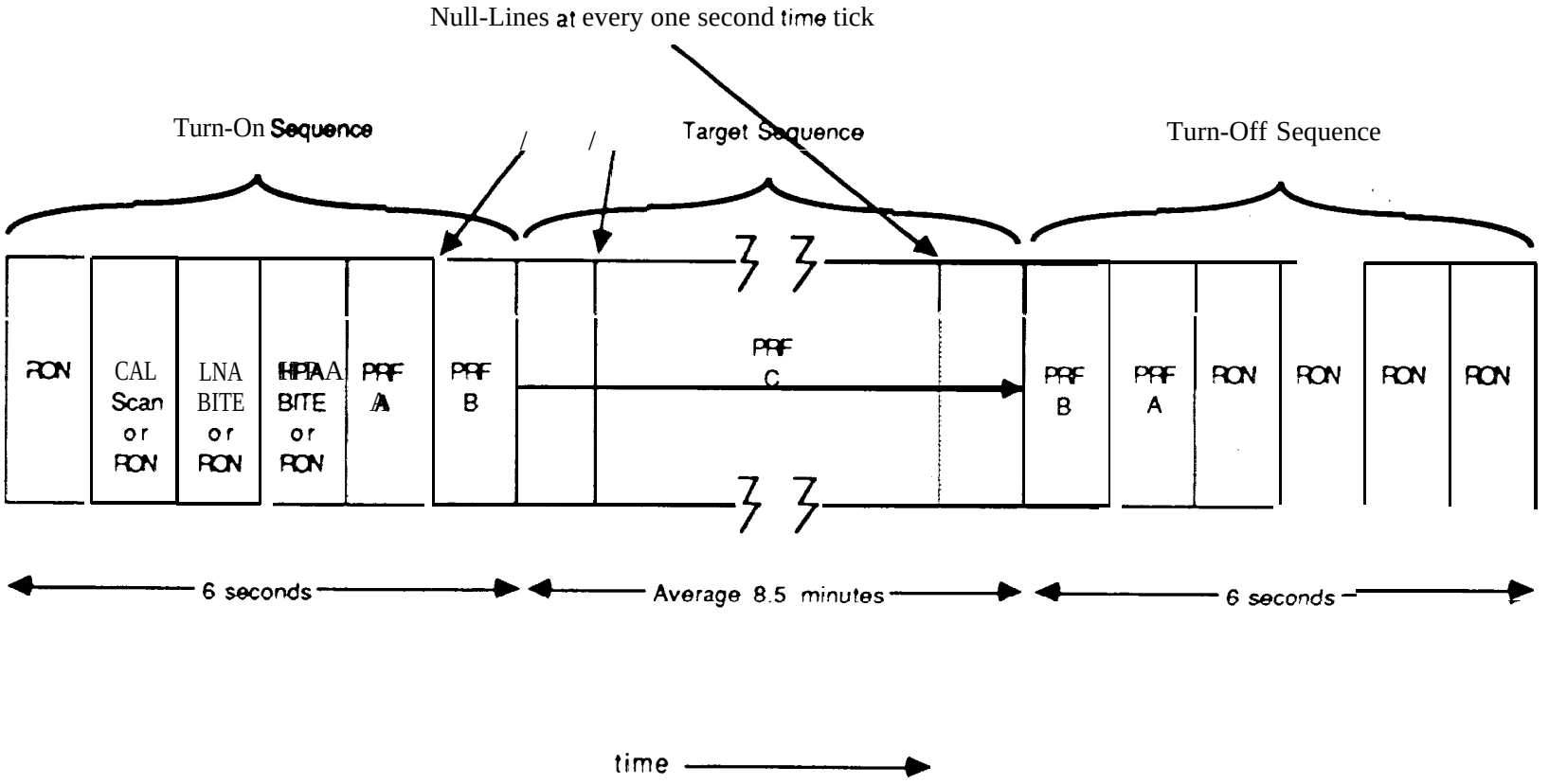

Fig. 3.1: SIR-C input data run format. Each segment in turn-on and turn-off sequence is 1 second duration.
RON: Receive Only Noise, LNA: Low Noise Amplifier, HPA: High Power Amplifier, CAL scan: Caltone Scan.

3.2 Data Products Definition

Operations of the SIR-C GDPS are planned as follows, where the key milestones are scheduled relative to the completion date of the mission, It is assumed that the tape duplications are done in the first two weeks post mission (at the KSC, not by the GDPS) and the first tape will be available to the GDPS team two week post mission. The SIR-C GDPS check-out will start two week post mission or upon the reception of the first tape and last for a 'period of six weeks. The Phase 1 operation will start upon the completion of GDPS check-out, or the beginning of the 9th week post mission, and continue until the end of the 20th week post mission for a period of twelve weeks. The Phase 2 operation will start upon the completion of Phase 1 operation, or the beginning of the 21st week post mission, and continue until four weeks prior to the second flight.

The SIR-C output data products include:

1. Image Data Product
   (a) Survey Image Product
   (b) Standard Multi-Look Detected Image Product
   (c) Standard Multi-Look Complex Image Product
   (d) Standard Single-Look Complex Image Product
2. Reformatted Signal Data Product.

The throughput requirements are as follows:

1. Phase 1 operation:
   Generate 24 Survey Image Products and 5 Standard Single-Look Complex Image Products per week.
2. Phase 2 operation:
   Generate 8.5 Multi-Look Detected Image products, 10.5 Multi-Look Complex Image Products, 1 Single-Look Complex Image Product, and 1 Reformatted Signal Data Product per week.

Image quality specifications including requirements and estimated performance of each output image product are shown in [5]. The data products are defined as follows:

1. Survey Image Product:

   (a) Description: strip image, 4-look, detected, deskewed, ground range, ~100 m resolution, 50 m pixel spacing, single-frequency, single-polarization

   (b) Data Format: S bits amplitude per pixel

   (c) Product Run Duration: entire data take with an S.5 minute average length (~ 3S00 Km)

   (d) Throughput: 24 runs per week for 12 weeks during Phase 1 operation

   (e) Medium: CD-ROM (distributed to PIs), CEOS formatted tape, strip thermal print image (the last two archived in the Radar Data Center, not for distribution to PIs)

2. Standard Multi-Look Detected Image Product

   (a) Description: frame image, multi-look, detected, deskewed, ground range, 12.5 m pixel spacing, 25 m resolution in azimuth, 25 m or natural resolution in range, single-frequency, single-polarization

   (b) Data Format: 16 bits amplitude per pixel

   (c) Product Run Duration: ~15 seconds (100 Km)

   (d) Throughput: S.5 runs per week for 40 weeks during Phase 2 operation

   (e) Medium: CEOS formatted tape, frame image print (the photoproduct is reduced from the digital product to fit onto a single print paper)

3. Standard Multi-Look Complex Image Product

   (a) Description: "frame image, multi-look, complex polarimetric data, deskewed, ground range, 12.5 m pixel spacing, 25 m resolution in azimuth, 25 m or natural resolution in range, single-frequency, dual-polarization or quad-polarization

   (b) Data Format: compressed cross-products, Dual-polarization: 5 bytes per pixel, Quad-polarization: 10 bytes per pixel

   (c) Product Run Duration: ~15 seconds (100 Km)

   (d) Throughput: 10.5 runs per week for 40 weeks during Phase 2 operation

   (e) Medium: CEOS formatted tape, frame image print (the photoproduct is reduced from the digital product to fit onto a single print paper)

4, Standard Single-Look Complex Image Product

(a) Description: frame image, single-look, complex, deskewed, slant range, natural spacing, full-resolution, single-frequency, all polarizations

(b) Data Format: compressed scattering matrix, Single-polarization: 4 bytes per pixel. . Ilual-polarization: 6 bytes pet pixel, Quad-polarization: 10 bytes per pixel

(c) Product Run Duration: $\sim$ 8 seconds (50 Km)

(d) Throughput: 5 rums per week for 12 weeks during Phase 1 operation, 1 run per week for 40 weeks during Phase 2 operation

(c) Medium: CEOS formatted tape, frame image print (the photoproduct is reduced from the digital product to fit onto a single print paper)

5. Reformatted Signal Data Product.

(a) Description: SAR signal data, radar, platform and processing parameters

(b) Data Format: 8 bit unpacked and DWP shifted data with original raw data header and CEOS standard header to include decoded parameter values

(c) Product Run Duration: $\sim$ 8 seconds (50 Km)

(d) Throughput: 1 run per week for 40 weeks during Phase 2 operation

(e) Medium: CEOS formatted tape

4. INITIAL PROCESSING PARAMETERS GENERATION ALGORITHM

The initial processing parameters generation algorithm is used to

(a) Generate initial Doppler parameters from the ephemeris data;

(b) Determine the-image latitude and longitude; and

(c) Generate parameters necessary to initiate the data processing and parameters used to interpret the image data.

The algorithm presented in this section is organized as follows: a) Definitions of coordinate systems, angles, rotations and radar attitude modes; b) Coordinate transformation; c) Initial Doppler predicts: d) Image latitude and longitude location determination; and e) Processing parameters and image parameters determination.

Let us use the following notations:

$R_s = (x_s, y_s, z_s)$: spacecraft position vector in the geocentric coordinate system;
$V_s = (Vx_s, Vy_s, Vz_s)$: spacecraft velocity vector in the geocentric coordinate system;
R_t: target position vector in the geocentric coordinate system;
V_t: target velocity vector in the geocentric coordinate system;
R_{st}: sensor-to-target position vector;
V_{st}: sensor-to-target velocity vector;
A_{st}: sensor-to-target acceleration vector;
R_e: earth radius at the equator;
R_p: earth radius at the polar region:
θ: longitude;
ϕ: latitude;
h: sensor altitude;
f_d: Doppler centroid frequency;
f_r: Doppler frequency rate;
λ: wavelength;
c: speed of light;
B: range chirp bandwidth;
PBW: processing bandwidth;
DWP: data window position;
n_p: number of pulses in the air;
f_s: range complex sampling rate;
N_r: number of range samples;
τ_d: electronic delay;
$\theta_R, \theta_Y, \theta_P$: roll, yaw and pitch rotation angles;
θ_T: antenna mechanical tilt angle;
θ_S: antenna electronic steering angle;
θ_L: antenna look angle;
θ_E: antenna elevation angle;
θ_A: azimuth squint angle;
r_{st}: slant range.

4.1 **Definitions**

4.1,1 **Spacecraft-Centered Local Coordinate System**

The origin of the spacecraft-centered local coordinate system is defined to be the center of the mass of the spacecraft. The Z-axis is pointing downward to the earth center, i.e..

$$u_z = -\frac{R_s}{|R_s|}$$

The Y-axis is pointing to the right, perpendicular to the plane determined by u_z and V_s, i.e.,

$$u_y = \frac{U^* \otimes V_s}{|u_z \otimes V_s|},$$

where "@" represents the cross-product (outer-product) operator. The X-axis completes the right-handed coordinate system, i.e,

$$U_r = u_y \otimes u_z .$$

4.1.2 Shuttle Body Coordinate System

The origin of the shuttle body coordinate system is defined to be the center of the mass of the space shuttle. The positive Z-axis is defined to be pointing downward. The positive X-axis is parallel to the vector from the center of mass to the nose of the space shuttle. The positive Y-axis is parallel to the right wing.

4.1.3 Geocentric **Coordinate Systems**

There are a number of geocentric coordinate systems used by the SIR-C. They include:

(a) Aries mean of 1950 coordinate system;

(b) Earth mean equator and equinox of epoch coordinate system; and

(c) Greenwich true of date coordinate system.

The first two coordinate systems are inertial, The last one is rotating, For the SIR-C, the Greenwich true of date coordinate system is used by the header subcommutated data. The Earth mean equator and equinox of epoch coordinate system is used by the MOS ephemeris file. The ephemeris parameters provided in the PATH tape are recorded in several coordinate systems. The Aeries mean of 1950 coordinate system will be used by the SIR-C.

The Aries mean of 1950 coordinate system is defined as follows:

Origin: The center of the Earth

Epoch: 2433282.423357 Julian date

X-Y plane: The mean equator of epoch

X-axis: Directed towards the mean of vernal equinox of epoch

Z-axis: Directed along the Earth's mean rotational axis and is positive north

Y-axis: Completes a right-handed coordinate system.

The Earth mean equator and equinox of epoch coordinate system is defined as follows:

Origin: The center of the Earth

Epoch: TBD Julian date, to be provided by the Mission Operations Subsystem

X-Y plane: The mean equator of epoch

X-axis: Directed towards the mean of vernal equinox of epoch

Z-axis: Directed along the Earth's mean rotational axis and is positive north

Y-axis: Completes a right-handed coordinate system.

The Greenwich true of date coordinate system is defined as follows:

Origin: The center of the Earth

X-Y plane: The Earth's true of date equator

X-axis: Directed towards the prime meridian

Z-axis: Directed along the Earth's true of date rotational axis and is positive north

Y-axis: Completes a right-handed coordinate system.

4.1.4 Earth Model

The Clarke 1866 oblate ellipsoid model is selected, which is

$$\frac{x^2 + y^2}{R_e^2} + \frac{z^2}{R_p^2} = 1 ,$$

where

$$R_e = 6378206.4 \text{ m}$$

$$R_p = 6356583.8 \text{ m}$$
$$f = \frac{1}{294.98}$$
$$e^2 = 2f \cdot \cdot f^2 = 0.006768658.$$

4.1.5 Roll, Yaw and Pitch Rotations

The roll is the rotation around the X-axis of the shuttle body with right rotation defined as the positive direction. The yaw is the rotation around the Z-axis of the shuttle body with right rotation defined as the positive direction. The pitch is the rotation around the }'-axis of the shuttle body with up rotation defined as the positive direction. For the SIR-C, the shuttle maneuver is confined to the rotation sequence of pitch-yaw-roll, The zero attitude is defined to be that the shuttle nose is directed forward and the shuttle bay is directed up away from the earth center. The attitude maneuver is controlled to provide a 26° angle between the positive Z-axis of the shuttle. body and the nadir vector.

4.1.6 Mechanical Tilt Angle

The mechanical tilt angle, θ_T, is defined to be the angle between the antenna panel and shuttle cargo bay (X-Y plane of the shuttle body). For the SIR-C, the antenna mechanical tilt is achieved by mechanically rotating the antenna about an axis fixed to the right hand side of the payload bay when facing forward. The mechanical tilt angle is fixed to be 14^o.

4.1.7 Electronic Steering Angle

The electronic steering angle, θ_S, is defined to be the angle between the antenna boresight vector and the vector perpendicular to the antenna panel. The downward steering is defined to be the positive direction, The maximum electronic steering angle is confined to be $\pm 23^o$.

4.1.8 Antenna Look Angle

The antenna look angle, θ_L, is defined to be the angle between the antenna boresight (peak gain) and the X-Z plane of the shuttle body.

4.1.9 Radar Attitude Modes

The SIR-C has two nominal radar attitude modes:

(a) Minus Z-Local-Vertical (- ZLV) mode or nose forward mode: nose aligned to the velocity vector, payload bay towards the earth center of mass, which results in a left-looking antenna; and

(b) Positive Z- Local-Vertical (+ ZLV) or tail forward mode: nose opposite to the velocity vector, payload bay towards the earth center of mass, which results in a right-looking antenna.

Under special conditions, the non-nominal attitude mode may be required, for which case the pitch, yaw and roll angles will be available to the processor.

These radar attitude modes results in right-looking and left-looking antenna. The right-looking image is adopted as the standard image display format. The flight direction is defined to be from left to right. The range direction is defined to be from top to bottom.

4.1.10 Effective Antenna Boresight Vector

The effective antenna boresight vector is determined by the mechanical tilt angle, electronic steering angle and shuttle attitude (pitch-yaw-roll rotation sequence).

4.1.11 **Off-Nadir Look Angle**

The off-nadir look angle is defined to be the angle between the antenna boresight vector and the nadir vector (the positive Z-axis of the spacecraft centered coordinate system). The positive elevation angle is defined to be right looking. For the SIR-C, following the mechanical tilt and shuttle attitude rotation, the antenna boresight is directed 40° off the nadir vector. With the electronic. steering angle, the resultant off-nadir look angle will range between $40 \pm 23°$.

4.1.12 **Azimuth Squint Angle**

The azimuth squint angle is defined to be the angle between the effective antenna boresight vector and the zero- Doppler hyperplane. The positive azimuth squint angle direction is defined to be forward (velocity direction).

4.2 Coordinate Transformation

4.2.1 Local and Geocentric Coordinate Transformation

The key step is to express the unit vectors of the local spacecraft-centered coordinate system in the geocentric. coordinate system.

$$u_z = \begin{pmatrix} u_{zx} \\ u_{zy} \\ u_{zz} \end{pmatrix} = \frac{-[x_s,\ y_s\ , z_s]^t}{|[x_s,\ y_s\ , z_s]^t|}$$

$$u_y = \begin{pmatrix} u_{yx} \\ u_{yy} \\ u_{yz} \end{pmatrix} = \frac{u_z \otimes [Vx_s, Vy_s\ , Vz_s]^t}{|u_z \otimes [Vx_s,\ Vy_s\ , Vz_s]^t|}$$

$$u_x = \begin{pmatrix} u_{xx} \\ u_{xy} \\ u_{xz} \end{pmatrix} = \frac{u_y \otimes u_z}{|u_y \otimes u_z|} .$$

Let (x', y', z') be a vector in the spacecraft-centered local coordinate system and (x, y, z) be the associated vector in the geocentric coordinate system. These two vectors are related by

$$\begin{pmatrix} x \\ y \\ z \end{pmatrix} = \begin{pmatrix} u_{xx} & u_{yx} & u_{zx} \\ u_{xy} & u_{yy} & u_{zy} \\ u_{xz} & u_{yz} & u_{zz} \end{pmatrix} \begin{pmatrix} x' \\ y' \\ z' \end{pmatrix} .$$

4.2.2 Polar and Cartesian Coordinate Transformation

4.2.2.1 Polar to Cartesian Coordinate Transformation

Let (x, y, z) be a vector in the Cartesian coordinate system. Let R be the magnitude of this vector, ϕ (latitude) be the angle between the vector and the X-Y plane and θ (longitude) be the angle between the projected vector on the X-Y plane and the positive X axis.

$$x = R\cos\phi\cos\theta$$

$$y = R\cos\phi\sin\theta$$

$$z = R\sin\phi .$$

4.2.2.2 **Cartesian to Polar Coordinate Transformation**

Again let (x_t, y_t, z_t) be a vector in the Cartesian coordinate system (a target on the earth surface). Let θ represent the longitude and the latitude. The local earth radius (from target to center of the earth) is

$$R_e =$$

The geocentric atitude is

$$\phi = \sin^{-1} \frac{z_t}{|R_t|} .$$

Positive ϕ means nor h latitude. Negative ϕ means south latitude. The longitude is

$$\theta = \begin{cases} \tan^{-1} \frac{y_t}{x_t} & \text{for } x_t \geq 0,\ y_t > 0 \\ 180^0 + \tan^{-1} \frac{y_t}{x_t} & \text{for } x_t < 0,\ y_t \geq 0 \\ -180^0 + \tan^{-1} \frac{y_t}{x_t} & \text{for } x_t \leq 0,\ y_t < 0 \\ \tan^{-1} \frac{y_t}{x_t} & \text{for } x_t > 0,\ y_t \leq 0. \end{cases}$$

Positive θ means east longitude, Negative θ means west longitude.

4.2.3 Geocentric and Geodetic Coordinate Transformation

Let ϕ be the geocentric latitude and ϕ_g the geodetic latitude. 'They are related by

$$\phi_g = \tan^{-1} \left[\frac{1}{(1 - e^2)} \tan \phi \right] .$$

4.2.4 Inertial and **Rotating** Coordinate **Transformation**

The inertial and rotating systems are related bv the angle between the two X-axis's or the conversion between the θ angle (longitude).

$$\begin{aligned} \theta_{inertial} &= \theta_{\text{rotating}} + \theta_{offset} \\ &= \theta_{rotating} + \theta_{ref} + w_e t , \end{aligned}$$

where $\theta_{inertial}$ is the longitude of the inertial coordinate system, $\theta_{rotating}$ the longitude of the rotating coordinate system, θ_{ref} the angle between the positive X-axis of the rotating system at a selected reference time and the inertial system, t the elapsed time in days since the reference time and w_e (= 360.98562960/day) the earth rotation rate.

4.3 Initial Doppler Predicts

4.3.1 Near Range Slant Range

Let us use the following notations:

i: range pixel index or azimuth line index, where $O \leq i \leq N_r - 1$;

$t_{min}(i)$: time since Doppler centroid that gives the minimum range migration;

$f_d(i)$: Doppler centroid of the ith azimuth line;

$f_r(i)$: Doppler frequency rate of the ith azimuth line, where $f_r(i) < O$;

l_1: length of the interpolator used for range migration compensation; and

l_2: length of the range interpolator used for geometric rectification.

The slant range, measured from the center of the aperture, of the first range sample prior to range compression is determined by the number of pulses in the air, data window position (DWP, including DWP fills) and electronic delay time.

$$R_0 = \left[\frac{n_p}{PRF} + DWP - \tau_d\right]\frac{c}{2}.$$

The slant range, measured from the center of the aperture, of the first range pixel following the range compression stays the same.

It can be shown that for each azimuth line,

$$t_{min} = \begin{cases} -\frac{f_d(i)}{f_r(i)}, & \text{if } |f_d(i)| < \frac{PRF}{2}; \\ +\frac{PRF}{2f_r(i)}, & \text{if } f_d(i) \leq -\frac{PRF}{2}; \\ -\frac{PRF}{2f_r(i)}, & \text{if } f_d(i) \geq \frac{PRF}{2}. \end{cases}$$

Let i_{min} be the minimum number of i such that

$$\frac{\lambda}{c/f_s}\left[f_d(i)t_{min} + \frac{1}{2}f_r(i)t_{min}^2\right] + i \geq \frac{l_1}{2} - 1.$$

The slant range, measured from the center of the aperture, of the. first range pixel following the azimuth compression is

$$R_1 = R_0 + i_{min}\frac{c}{2f_s}$$

and the slant range, measured from the flight track, is

$$R_1' = R_1 - \frac{\lambda f_d^2(i_{\min})}{4|f_r(i_{\min})|} .$$

The slant range. measured from the center of the aperture, of the first range pixel following the geometric rectification is

$$\begin{aligned} R_2 &= R_0 + i'_{\min}\frac{c}{2f_s} \\ &= R_0 + \left(i_{\min} + \frac{l_2}{2} - 1\right)\frac{c}{2f_s} \end{aligned}$$

and the slant range, measured from the flight track, is

$$R_2' = R_2 - \frac{\lambda f_d^2(i'_{\min})}{4|f_r(i'_{\min})|} .$$

4.3.2 Antenna Look Angle

The antenna look angle prior to shuttle rotation is

$$\theta_L = \theta_T + \theta_S .$$

4.3.3 Antenna Unit Pointing Vector

The antenna unit pointing vector prior to shuttle rotation is

$$p^o = \begin{pmatrix} 0 \\ \sin\theta_L \\ -\cos\theta_L \end{pmatrix}$$

The pointing vector following the shuttle pitch-yaw-roll rotation sequence becomes

$$\begin{aligned} p' &= \begin{pmatrix} \cos\theta_P & 0 & \sin\theta_P \\ 0 & 1 & 0 \\ -\sin\theta_P & 0 & \cos\theta_P \end{pmatrix} \begin{pmatrix} \cos\theta_Y & -\sin\theta_Y & 0 \\ \sin\theta_Y & \cos\theta_Y & 0 \\ 0 & 0 & 1 \end{pmatrix} \begin{pmatrix} 1 & 0 & 0 \\ 0 & \cos\theta_R & -\sin\theta_R \\ 0 & \sin\theta_R & \cos\theta_R \end{pmatrix} p^o \\ &= \begin{pmatrix} p'_x \\ p'_y \\ p'_z \end{pmatrix} . \end{aligned}$$

4.3.4 Off-Nadir Look Angle

The off-nadir look angle is

$$\theta_E = \mathrm{Cos}^{-1} p'_z .$$

4.3.5 Left-Looking and Right-Looking

If $p'_y > 0$. the antenna is tight-looking. Else, it is left-looking.

4.3.6 Azimuth **Squint Angle**

The azimuth squint angle is approximately

$$\theta_A = \sin^{-1} p'_x .$$

4.3.7 Range Equation Solution

Let us transform the unit pointing vector from the local spacecraft-centered coordinate into the earth-centered coordinate system.

$$p = \begin{pmatrix} p_x \\ p_y \\ p_z \end{pmatrix} = T \begin{pmatrix} p'_x \\ p'_y \\ p'_z \end{pmatrix} = \begin{pmatrix} u_x & u_y & u_z \end{pmatrix} \begin{pmatrix} p'_x \\ p'_y \\ p'_z \end{pmatrix} .$$

where T represents the transformation. Normalize p

$$p = \frac{p}{|p|} .$$

The target position is expressed as

$$\begin{aligned} R_t &= \begin{pmatrix} x_t \\ y_t \\ z_t \end{pmatrix} \\ &= R_s + R\,p \\ &= \begin{pmatrix} x_s \\ y_s \\ z_s \end{pmatrix} + R \begin{pmatrix} p_x \\ p_y \\ p_z \end{pmatrix} . \end{aligned}$$

where R, representing the slant range, is determined as follows.

$$\frac{(x_s + R\,p_x)^2 + (y_s + R\,p_y)^2}{R_e^2} + \frac{(z_s + R\,p_z)^2}{R_p^2} = 1$$

Reformulate the equation. We have the following quadratic equation

$$\left(\frac{p_x^2 + p_y^2}{R_e^2} + \frac{p_z^2}{R_p^2}\right) R^2 + \left(\frac{2p_x x_s + 2p_y y_s}{R_e^2} + \frac{2p_z z_s}{R_p^2}\right) R + \left(\frac{x_s^2 + y_s^2}{R_e^2} + \frac{z_s^2}{R_p^2} - 1\right) = 0$$

or

$$AR^2 + BR + C = 0 .$$

The slant range is

$$R = \frac{-B - \sqrt{B^2 - 4AC}}{2A} .$$

The target velocity is

$$V_t = \begin{pmatrix} -y_t w_e \\ x_t w_e \\ 0 \end{pmatrix} . \quad w_e = \text{angular velocity of Earth}$$

Calculate the slant range error

$$\mathrm{AR} = r_{sl} - R$$

The associated elevation angle difference is approximately

$$\Delta\theta_E = \frac{\Delta R}{(\tan\theta_I)R} ,$$

where the incidence angle is

$$\theta_I = 180^\circ - \cos^{-1}\frac{r_{sl}^2 + |R_t|^2 - (|R_n| + h)^2}{2r_{sl}|R_t|} ,$$

with $|R_t|$ and $|R_n|$ representing the earth radius at the target and the nadir respectively,

Update the look angle

$$\theta_L = \theta_L + (\mathrm{sgn})\Delta\theta_E ,$$

where "sgn = +" for both nose-forward and tail-forward attitude modes.

The new look angle is used to regenerate the antenna pointing vector and solve the range equation iteratively until ΔR is less than a preset threshold.

4.3.8 Doppler Parameter Calculation

The Doppler centroid is

$$f_d = -\frac{2V_{st} \bullet R_{st}}{\lambda |R_{st}|},$$

where " $\bullet$" represents the dot-product (inner-product) operator, The Doppler frequency rate is

$$f_r = -\frac{2(|V_{st}|^2 + R_{st} \bullet A_{st})}{\lambda |R_{st}|}.$$

The same procedure is repeated to generate the Doppler parameters across the range. These parameters are quadratic fit in range to generate three polynomial coefficients: constant, linear and quadratic.

4.4 Image Geodetic Location

The image location is determined by solving the range-Doppler equations. The given parameters are sensor position/velocity vector, slant range, earth model and processing Doppler centroid frequency

4.4.1 Range-Doppler Equation Solution

An approach to solve the range-Doppler equations is summarized as follows:

Range loop:

a) Determine the target position vector based on the the antenna pointing vector;

b) Calculate the slant range error;

c) Translate the slant range error into the look angle;

d) Update the an enna pointing vector;

e) Iterate a) to d until the slant range error is less than a preset threshold:

Azimuth loop:

f) Calculate the Doppler frequency based on the sensor and target state vectors;

g) Calculate the Doppler frequency errors at near and far range. If the Doppler errors are less than a preset threshold, stop. Else, continue.

h) Translate the Doppler frequency errors into yaw and pitch angles;

i) Update the antenna pointing vector;

j) Go to the range loop.

One approach to solve the range equation is shown in Section 4.3,7. In the following we discuss an approach to solve the Doppler equation.

4.4.2 Doppler Equation Solution

Let f_d represents the Doppler centroid estimate obtained from the clutterlock algorithm and f_d^o the Doppler based on the sensor and target state vectors. The Doppler frequency difference is

$$\Delta f_d = f_d - f_d^o$$

$$= \frac{2|V_{st}|}{\lambda} \sin \Delta\theta_A$$
$$\sim \frac{2|V_{st}|}{\lambda} \Delta\theta_A$$

By using the near and far range Doppler errors the yaw and pitch angles can be obtained.

Recall that the antenna pointing vector is

$$p' = \begin{pmatrix} p'_x \\ p'_{yy} \\ p'_z \end{pmatrix} .$$

Following the rotation of small yaw and pitch, the new antenna pointing vector is approximately

$$p' = \begin{pmatrix} 1 & -\Delta\theta_Y & 0 \\ \Delta\theta_Y & 1 & 0 \\ 0 & 0 & 1 \end{pmatrix} \begin{pmatrix} 1 & 0 & \Delta\theta_P \\ 0 & 1 & 0 \\ -\Delta\theta_P & 0 & 1 \end{pmatrix} \begin{pmatrix} p'_x \\ p'_y \\ p'_z \end{pmatrix}$$
$$= \begin{pmatrix} 1 & -\Delta\theta_Y & \Delta\theta_P \\ \Delta\theta_Y & 1 & 0 \\ -\Delta\theta_P & 0 & 1 \end{pmatrix} \begin{pmatrix} p'_x \\ p'_y \\ p'_z \end{pmatrix}$$
$$= \begin{pmatrix} p'_x - \Delta\theta_Y\, p'_y + \Delta\theta_P\, p'_z \\ \Delta\theta_Y\, p'_x + p'_y \\ -\Delta\theta_P\, p'_x + p'_z \end{pmatrix}$$

For small yaw and pitch errors, the azimuth squint angle can be approximated by

$$\Delta\theta_A = \Delta p'_x$$
$$= -\Delta\theta_Y\, p'_y + \Delta\theta_P\, p'_z$$

So, the yaw and pitch angles can be solved by the two equations

$$(-p'_y)\Delta\theta_Y + (p'_z)\Delta\theta_P = \quad -$$

established at near and far range. The yaw and pitch angles are then used to rotate the antenna pointing vector.

4.5 Other Processing And Image Related Parameters

4,5.] Resolution and Pixel Spacing

The slant range resolution is

$$\delta_r = k_r \frac{c}{2B},$$

where c represents the speed of light and B the range chirp bandwidth and k_r the range broadening factor. The ground range resolution is

$$\delta_r = k_r \frac{c}{2B(\sin\theta_I)},$$

where θ_I represents the incidence angle. The azimuth resolution is

$$\delta_a = k_a \frac{V_{sw}}{PBW},$$

where V_{sw} represents the swath velocity, PBW the azimuth processing bandwidth and k_a the azimuth broadening factor. The processing bandwidth is generated as a function of PRF to meet the azimuth ambiguity requirement.

The natural range pixel spacing is

$$\Delta r = \frac{c}{2f_s},$$

where f_s represents the range complex sampling rate. The natural azimuth pixel spacing is

$$\Delta x = \frac{V_{sw}}{PRF}.$$

For the SIR-C standard processor, there are three standard image products:

(a) Single-Look Complex Image Product;

(b) Multi-Look Detected Image Product; and

(c) Multi-Look Complex Image Product.

The Single-Look Complex Image Product is represented in the slant range domain. The Multi-Look Image Product will be resampled to equal spacing in the ground range domain. The azimuth resolution is selected to be 25 meter and the range resolution is either 25 m or natural if greater than 25 m. The pixel spacing is selected to be 12.5 m.

4.5.2 **Swath Truncation**

The procedure to determine the SNR swath width is as follows:

(a) Determine the illumination swath width based on the SNR estimate and range antenna pattern. A 6 dB SNR end-to-end variation will be adopted as the default cut-off value., An option is reserved for manual cut-off value,

(b) Determine the data rate limit swath based on the data rate, PRF, pixel spacing and target incidence angle.

(c) The effective swath width is the minimum of the two swath widths.

4.5.3 Swath Velocity

The swath velocity is

$$V_{su} = |V_s - V_t| \frac{|R_t|}{|R_n| + h} \cos(\theta_I - \theta_E),$$

where $|R_t|$ and $|R_n|$ represent the local earth radius at the image center and the nadir respectively and h the sensor altitude.

4.5.4 Incidence Angle

The incidence angle is

$$\theta_I = 180^\circ - \cos^{-1} \frac{r_{sl}^2 + |R_t|^2 - (|R_n| + h)^2}{2 r_{sl} |R_t|}.$$

4.5.5 **Azimuth Squint** Angle

The azimuth squint **angle is** approximately

$$\theta_A = \sin^{-1} \left(\frac{\lambda f_d}{2|V_{st}|} \right).$$

4.5.6 **Track** Angle

The track angle is defined to be the angle between the swath velocity and the local north direction. It is derived as follows. The local east direction is

$$u_E = \frac{\begin{pmatrix} 0 \\ 0 \\ 1 \end{pmatrix} \otimes R_t}{\left| \begin{pmatrix} 0 \\ 0 \\ 1 \end{pmatrix} \otimes R_t \right|}$$

and the local north direction is

$$u_N = \frac{R_t \otimes u_E}{|R_t \otimes u_E|},$$

The local track vector (or equivalently the track angle) is

$$u_T = \begin{pmatrix} u_E^t \\ u_N^t \end{pmatrix} \frac{V_{st}}{|V_{st}|},$$

where superscript "t" represents transposition

4.5.7 Illumination Angle

The illumination vector (or equivalently the illumination angle) is defined to be the projection of the effective antenna boresight vector on the u_E-u_N plane. It is calculated as follows.

$$u_I = \begin{pmatrix} u_E^t \\ u_N^t \end{pmatrix} p.$$

5. TURN-ON AND TURN-OFF SEQUENCE PROCESSING ALGORITHM

The turn-on and turn-off sequence data are inserted at the beginning and end of each data take. They are used for radiometric calibration and PRF ambiguity resolution purpose.

The BITE turn-on sequence data consists of the following data segments for a total of seven seconds. The first second of the PRF_C data is included for PRF ambiguity resolution.

(a) One second Receive Only Noise data;

(b) One second Caltone Scan data;

(c) One second LNA data;

(d) One second HPA data;

(e) One second PRF_A data;

(f) One second PRF_B data;

(g) One second PRF_C data.

The no-BITE turn-on sequence data consists of the following data segments for a total of seven seconds.

(a) Four seconds Receive Only Noise data;

(b) One second PRF_A data;

(c) One second PRF_B data;

(d) One second PRF_C data.

The turn-off sequence data consists of the following data segments for a total of seven seconds. The last second of the PRF_C data is included for PRF ambiguity resolution,

(a) one second PRF_c data;

(b) One second PRF_B data;

(c) One second PRF_A data;

(d) Four second Receive Only Noise data.

The PRF (except for the PRF scan data), radar mode and data representation of the turn-on and turn-off sequence data are the same as those of the nominal data take. All the channels

of the receive only noise data and the caltone scan data will be processed for parameter estimation. The LNA and the HPA BITE data will be saved to disk files and prosed to the Calibration Subsystem for further processing. For the PRF scan data, only the channel selected for survey processing is processed to resolve the PRF ambiguity.

5.1 Receive Only Noise

The Receive Only Noise (RON) data is used to estimate the noise power and the processor noise data gain. The processor noise data gain is used for absolute calibration. It is only computed for a limited number of data takes.

The procedure to estimate the noise power is as follows.

(a) Estimate the noise power by calculating the mean power of the data samples acquired during the turn-on and turn-off RON period.

The procedure to estimate the processor noise data gain is as follows.

(a) I'recess the RON data of the turn-off sequence into image data using the reference functions and window functions employed by the standard processor;

(b) Calculate the power of this image (processed noise) data; and

(c) Calculate the processor noise data gain, which is established as the ratio of the noise power after and before the data processing.

For the SIR-C processor, a block of 512 by 512 samples per polarization is sufficient to derive a noise power estimate with an uncertainty less than 0.12 dB.

5.2 Caltone Scan

The calibration tone is injected into the front end of the SIR-C receive electronics (excluding the antenna). It is coherent with the PRF and is set 6 dB below the expected signal level during the data take and 6 dB below the full scale of ADC during the turn-on sequence. The caltone scan data consists of 11 caltone frequency positions with the oscillator dwelling on each position for 64 pulses, independent of the PRF value. The caltone scan data are used to estimate the gain variation across the range spectrum.

The caltone scan data processing procedure is described as follows.

(a) Separate the relevant cal tone scan data into 11 segments each of a unique caltone frequency:

(b) Perform coherent sum of the range line data within each segment;

(c) Pad the range line data by the remaining caltone signal;

(d) Fourier transform the sum of the range line data to obtain range spectra; and

(e) Estimate the caltone gain and phase from the correct FFT bin of each segment.

For the SIR-C processor, it is sufficient to use the 2048-point real FFT ancl 16 range lines. This will induce a gain estimation uncertainty less than 0.01 dB and a phase uncertainty less than 1 degree.

5.3 PRF Scan

The PRF scan data consists of three seconds of data, each acquired using a distinct PRF. These data are used to resolve the PRF ambiguity caused by a large antenna pointing error.

The PRF ambiguity is resolved in three steps:

(a) Estimate the ambiguous Doppler centroid as a function of range for each PRF;

(b) Resolve the ambiguity as a function of range using these three ambiguous Doppler centroid estimates; and

(c) Regenerate the (unambiguous) Doppler centroid frequency for the PRF_C segment as a function of range. Apply a quadratic fit in range. Discard the outliers which occur in the range fit.

5.3.1 Ambiguous Doppler Centroid Estimation

Since the Doppler drift characteristics and synthetic aperture length are different for I,-band and C-band, the procedure to estimate the Doppler centroid is discussed separately below.

5.3. I. I C-Band

For the C-band, the standard preprocessing (clutterlock) algorithm is applied to estimate the Doppler centroid of each data segment as follows.

(a) Range compress the data using one quarter of the range chirp bandwidth. The following range FFT length is selected:

Single-polarization: 16K real forward FFT and 2 K complex inverse FFT;

Dual-polarization: 8 K real forward FFT and 1 K complex inverse FFT;

Quad-polarization: 4 K real forward FFT and 512 complex inverse FFT;

(b) Azimuth compress the data using full synthetic aperture, L_a. Following the azimuth compression, only the first $PRF - L_a$ azimuth pixels are retained. The azimuth FFT length is selected to be 2 K;

(c) Fourier transform the azimuth compressed data in azimuth (good data points only) using 1 K FFT;

(d) Energy detect and average the azimuth spectra;

(e) Apply the energy balancing technique to estimate the Doppler centroid; and

(f) Iterate (b) to (e) until the estimate converges.

5.3.1.2 **I.-Band .**

For the I.-band, the Doppler centroid is estimated using the azimuth spectra of the range compressed data as follows.

(a) Range compress the data using one quarter of the range bandwidth;

(t)) Fourier transform the data in azimuth using 2KFFT;

(c) Energy detect and average the azimuth spectra; and

(d) Apply the energy balancing technique to estimate the Doppler centroid.

5.3.2 **PRF** Ambiguity Resolution

Let PRF_A, PRF_B, and PRF_C be the three PRFs used to resolve the DCE ambiguity. It is assumed that the radar sequentially dwells on PRF_A first, then PRF_B and PRF_C and remains on PRF_C for collection of the science data. The PRF_A and PRF_B represent two additional PRFs employed solely to resolve the DCE ambiguity. Let $\hat{f}_{dA}$, $\hat{f}_{dB}$, and $\hat{f}_{dC}$ be three ambiguous Doppler centroid estimates (the baseband Doppler centroid frequencies), where $O \leq \hat{f}_{dA} < PRF_A$, $O \leq \hat{f}_{dB} < PRF_B$, and $O \leq \hat{f}_{dC} < PRF_C$. These ambiguous estimates are obtained from the clutterlock algorithm.

Let f_{dA}, f_{dB}, and f_{dC} be the unambiguous Doppler centroid estimates for these three unique PRFs. We now have

$$
\begin{aligned}
f_{dA} &= k_A PRF_A + \hat{f}_{dA} \\
f_{dB} &= k_B PRF_B + \hat{f}_{dB} \\
f_{dC} &= k_C PRF_C + \hat{f}_{dC} \quad ,
\end{aligned}
$$

where k_A, k_B, and k_C represent the ambiguity number. Ideally $f_{dA} = f_{dB} = f_{dC}$. However, due to the DCE error and attitude drift, these three parameters become random numbers. The effect of the antenna drift rate can be partially compensated by utilizing the information provided by the on-board attitude sensors, reducing the variance among f_{dA}, f_{dB} and f_{dC} to

factors only due to the DCE error and the unmodeled attitude drift. If we select the center time of the block of the data used to estimate $\hat{f}_{dC}$ as a reference, we can redefine

$$\hat{f}_{dA} \leftarrow \hat{f}_{dA} - d_A^o - d_B^o$$
$$\hat{f}_{dB} \leftarrow \hat{f}_{dB} - d_B^o \ ,$$

where d_A^o represents the Doppler drift between PRF_A and PRF_B and d_B^o the drift between PRF_B and PRF_C. Since' the radar is assumed to operate in order of PRF_A, PRF_B and PRF_C, the Doppler centroid estimate of PRF_C is chosen as the initial Doppler estimate to reduce the potential Doppler drift error from the time the Doppler is estimated to the time the Doppler is applied in data processing.

Let (f_{dmin}, f_{dmax}) represent the interval of the Doppler centroid frequency error realized at the worst case attitude error.

Under certain conditions, i.e., when the Doppler error is small compared to the PRF difference, an efficient approach can be used to quickly resolve the ambiguity as shown in the following algorithm.

Fast Ambiguity Resolution Algorithm for PRFs of Arbitrary Numerical Values

Let

$$\text{APRF} = PRF_C - PRF_B$$
$$m_B = \frac{PRF_B}{\Delta PRF} \ ,$$

where m_B is a real number. It can be shown

$$f_{dC}(i) = k_C(i) \times PRF_C + \hat{f}_{dC}$$
$$k_C(i) = \text{rnd}\left[\frac{\hat{f}_{dB} - \hat{f}_{dC}}{\Delta PRF} + i \times m_B\right] \ ,$$

where "rnd" represents the integer round-off operation. Since for a given i,

$$k_B(i) = k_C(i) + i \ ,$$

we can write

$$\delta_A = [f_{dC}(i) - \hat{f}_{dA}] \bmod PRF_A$$

$$\delta_B = f_{dC}(i) - [k_B(i)\, PRF_B + \hat{f}_{dB}]$$

where it is chosen such that $|\delta_A| \leq PRF_B/2$ and $|\delta_B| \leq PRF_C/2$ and the optimal i is the one that minimizes

$$\delta = \sqrt{\delta_A^2 + \delta_B^2} \ .$$

We can then determine $\hat{k}_A$ from

$$\hat{k}_A(i) = \frac{f_{dC}(\hat{i}) - \hat{f}_{dA}}{PRF_A}$$

which gives us the' unambiguous estimates

$$f_{dA} = \hat{k}_A PRF_A + \hat{f}_{dA}$$
$$f_{dB} = \hat{k}_B PRF_B + \hat{f}_{dB}$$
$$f_{dC} = \hat{k}_C PRF_C + \hat{f}_{dC} \ .$$

##

The key step of the algorithm is the calculation of $k_C(i)$. It indicates that to quickly resolve the ambiguity using the above algorithm, the error in $\hat{f}_{dB} - \hat{f}_{dC}$ must be smaller than one-half of $\triangle PRF$.

6. SURVEY PROCESSING ALGORITHM

The SIR-C survey processing algorithm is a burst mode processing algorithm. To attain high throughput rate, the data is bursted in the azimuth direction with a duty cycle factor equal to one quarter (and one half as a limited option). The data volume is further reduced in the range direction using one quarter of the range bandwidth in the range compression. The azimuth compression is performed using the deramp FFT processing algorithm, also known as the spectral analysis (SPECAN) algorithm. Following the azimuth compression, the along-track radiometric compensation is used to compensate the scalloping effects and the geometric rectification is used for fanshape resampling, slant-to-ground range conversion before the burst images are overlayed into a strip image. Fig. 6.1 shows the survey processing algorithm flowchart.

The initial Doppler centroid frequency is obtained from processing the PRF scan data recorded in the turn-on sequence at the start of each data take. This Doppler centroid frequency is tracked by a burst mode clutterlock algorithm during the data processing. At the end of data processing, the tracking accuracy is verified by comparing the Doppler centroid frequency to that obtained from processing the PRF scan data recorded in the turn-off sequence. Since the burst data volume is too small to produce an accurate Doppler frequency rate estimate, the Doppler frequency rate is directly derived from the ephemeris data.

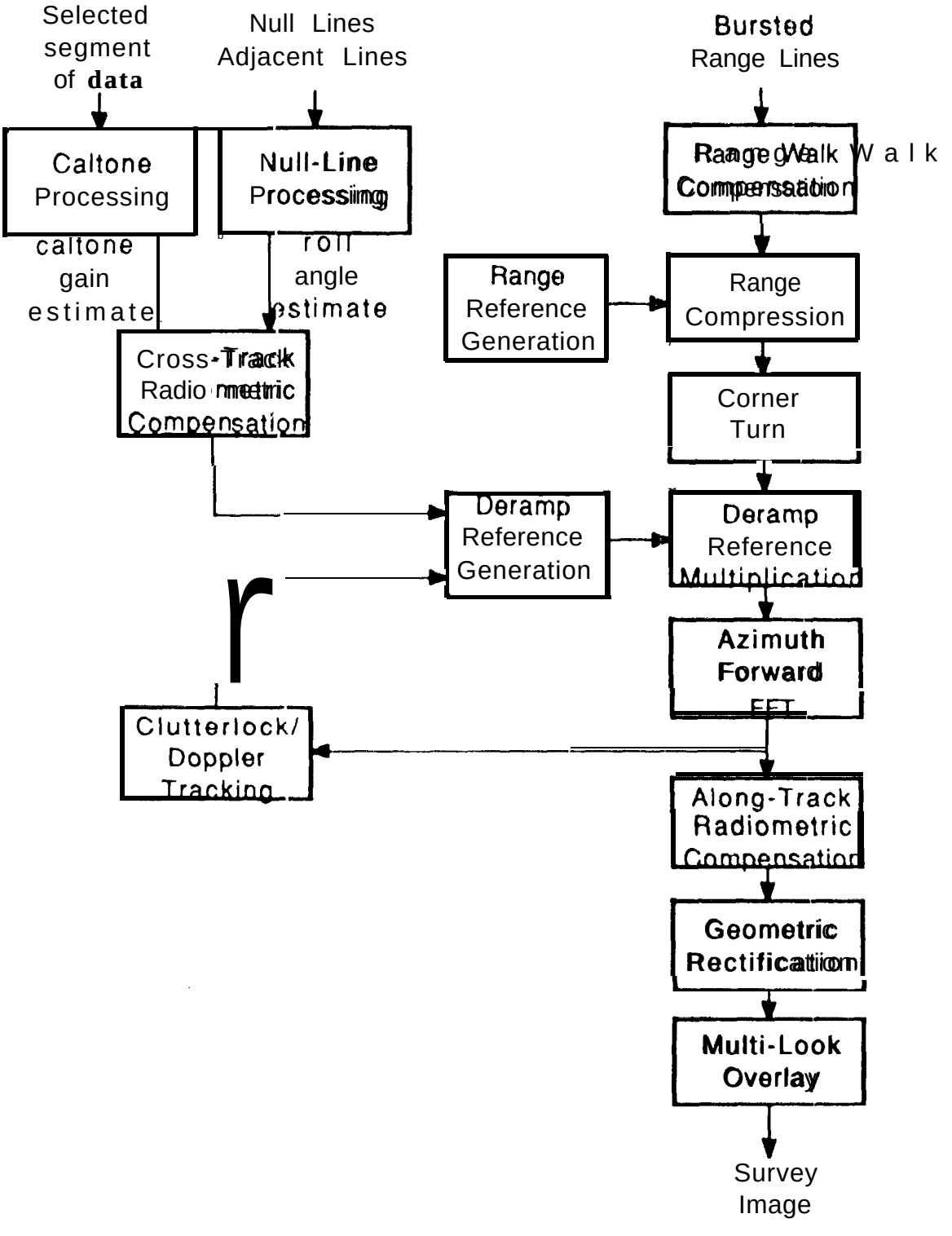

Fig. 6.1: Survey processing algorithm flowchart.

Let us use the following notations:

L_a: full synthetic aperture length;
L_b: burst length;
p: burst period:
d: duty cycle;
n_L: number of looks;
s: range presum factor;
N_a: deramp FFT length;
δ_a: azimuth resolution;
δ_r: range resolution:
f_d: Doppler centroid frequent];
f_r: Doppler frequency rate, f_r < O;
PBW: full azimuth processing bandwidth;
T: full synthetic aperture time;
B: range chirp bandwidth;
τ: pulse duration;
f_s: range complex sampling rate;
b_0: range chirp rate;
c: speed of light;
λ: wavelength;
L_r: range reference function length;
V_{st}: sensor-to-target relative velocity;
Δr: output range pixel spacing;
Δx: output azimuth pixel spacing;
L: antenna length;
R_{en}: Radius of the earth at the nadir;
R_{et}: Radius of the earth at the mid-swath;
r_{sl}: near range slant range;
R_g: near range ground range;
h: spacecraft altitude;
θ: azimuth squint angle;
V_s: spacecraft velocity in the earth body fixed coordinate system;
V_{sw}: swath velocity;
n: processing block index, where $n \geq$ O;
i: range pixel index before geometric rectification;

r': range pixel index after geometric rectification;

k: azimuth pixel index before geometric rectification:

k': azimuth pixel index after geometric rectification;

C_1: distance in the along-track direction;

C_2: distance in the cross-track direction;

$f_d^{[n]}(i)$: Doppler centroid frequency of the ith range pixel in the nth block;

$f_r^{[n]}(i)$: Doppler frequency rate of the ith range pixel in the nth block, where $f_r^{[n]}(i) < 0$;

$f_{dm}^{[n]}$: Doppler centroid frequency at the mid-swath in the nth block;

$f_{rm}^{[n]}$: Doppler frequency rate at 'the mid-swath in the nth block, where $f_{rm}^{[n]} < 0$.

6.1 Burst Design

The azimuth resolution is determined by the burst length.

$$\delta_a = k_a \frac{V_{sw}}{\frac{L_b}{PRF}|f_r|},$$

where k_a represents the broadening factor. The equivalent number of looks is determined by the number of bursts in the full synthetic aperture.

$$n_L = \frac{L_a}{p}.$$

For the SIR-C survey processor, the baseline design parameters are selected as follows.

a) $L_b = L_a/16$;

b) $p = L_a/4$;

c) $d = 1/4$;

d) $n_L = 4$; and

e) $\delta_a = 16\delta_a^o$, where δ_a^o represents the full azimuth resolution.

The data is bursted in the azimuth direction, i.e., the first L_b range lines are transmitted and the next $3L_b$ range lines are suppressed, and so on. The same burst operation is repeated until the end of data run. Some limited number of survey runs will be processed by doubling the range and the azimuth processing bandwidths to produce a higher resolution image.

6.2 **Range Walk Compensation**

The range walk compensation is done in the time domain prior to range compression. No interpolation is employed. The precision of the range walk compensation is one half of the input range sample" spacing. Let f_{dm} be the Doppler centroid at the mid-swath. Also let "rnd" represent the round-off operation. If f_{dm} <0, for the kth range line, start reading the data from the ith sample, where

$$i = \text{rnd}\left[\frac{\lambda|f_{dm}|\frac{(k-1)}{PRF}}{\frac{c}{2f_s}}\right],$$

for $1 \leq k \leq L_b$, L_b representing the number of pulses in a burst. If $f_{dm} > 0$, for the kth range line, start reading the data from the ith sample, where

$$i = \text{rnd}\left[\frac{\lambda|f_{dm}|\frac{(L_b-k)}{PRF}}{\frac{c}{2f_s}}\right]$$

Recall that the input sample is real for the SIR-C and $2f_s$ represents the real data sampling rate. The range walk compensation indices are initialized for every burst of data.

6.3 Range Compression

6.3.1 Range Reference Function

The range reference function for the theoretical range chirp is generated in the time domain using full range chirp bandwidth.

$$H(f) = \mathcal{F}\{h(r)\}$$
$$h(r) = e^{j\phi(r)}$$
$$\phi(r) = 2\pi\left[f_0\frac{r}{f_s} + \frac{1}{2}b_0\left(\frac{r}{f_s}\right)^2\right],$$

for $0 \le r \le L_r - 1$, where

$$L_r = f_s\tau$$
$$b_0 = \pm\frac{B}{\tau}$$
$$f_0 = \frac{f_s \mp B}{2},$$

for up-chirp and down-chirp respectively. The SIR-C uses the clown-chirp,

The spikes in the range spectrum, caused by caltone signals and interference signals, are suppressed. The existence of spikes in the range spectrum produces bright skewed lines while the deramp FFT processing algorithm is used as the azimuth compression algorithm.

Only one quarter of the range bandwidth is used in the reference function multiplication. The portion of the range spectrum (the range processing spectrum) is selected to minimize the effects of strong spike signals.

The cosine squared plus pedestal function is selected as the weighting function to control the sidelobe ratios. The pedestal height is selected to be 0.45. The weighting function is generated and multiplied with the reference function in the frequency domain.

No secondary range compression is required. This results in a Doppler independent range reference function. Thus, no range reference function update is required to accommodate the Doppler drift.

6.3.2 Range Compression

The range compression is accomplished in five steps:

(a) Range FFT each range line;

(b) Locate the data within the range processing spectrum;

(c) Range reference function multiplication;

(d) Baseband shift; and

(e) Range inverse FFT.

The range FFT length is selected as follows.

(a) Single-polarization: forward FFT: 16 K real and inverse FFT: 2 K complex;

(b) Dual-polarization: forward FFT: 8 K real and inverse FFT: 1 K complex;

(c) Quad-polarization: forward FFT: 4 K real and inverse FFT: 512 complex.

6.4 Azimuth Compression

6.4.1 Deramp Reference Function

The deramp reference function, representing the azimuth reference function, is generated in the time domain. Since there is severe Doppler drift in both along-track and cross-track directions, the azimuth reference function must be updated accordingly. The azimuth reference function is updated every processing block in the along-track direct ion." In the cross-track direction, it is updated according to the specified update rate. The azimuth reference function length, equal to the burst length, is maintained constant in both along-track and cross-track directions. This results in a variable azimuth resolution in the range direction.

The azimuth reference function is generated as follows.

$$R(x) = e^{j\phi(x)},$$

where

$$\phi(x) = 2\pi\left[\left(\frac{PRF}{2} - f_d\right)\left(\frac{x - \frac{L_b}{2}}{PRF}\right) + 0.5|f_r|\left(\frac{x - \frac{L_b}{2}}{PRF}\right)^2\right],$$

for $0 \leq x \leq L_b - 1$, where $f_r < 0$. The f_r term compensates the quadratic phase term of the point-target phase history, The $PRF/2 - f_d$ term shifts the antenna boresight to the center . of the burst image.

Again, the cosine squared plus pedestal function is selected as the weighting function to control the sidelobe ratios. 'I'he pedestal height is selected to be 0.45. The weighting function is generated and multiplied with the reference function in the time domain.

The cross-track radiometric correction vector is generated based on the range antenna pattern, slant range, incidence angle, caltone gain estimates and the range pixel shift as a result of the shuttle roll angle drift. This correction vector is multiplied with the azimuth reference function in the cross-track direction.

6.4.2 Azimuth Compression

The deramp FFT processing algorithm is used as the azimuth compression algorithm. The

azimuth FFT length, N_a, is selected to be the minimum power of 2 that is greater than or equal to L_b. The azimuth compression is accomplished in four steps:

(a) Multiply (no complex conjugate) the range compressed data by the deramp reference function in azimuth;

(b) Zero pad the data to the azimuth FFT length; and

(c) Forward azimuth FFT the data.

6.5 Along-Track Radiometric Compensation

Following the deramp processing, the intensity of the data in the along-track direction is the product of the target backscatter coefficients and the azimuth antenna pattern. This azimuth antenna pattern modulation phenomenon is also known as the scalloping effect. Radiometric compensation is needed to remove this scalloping effect.

Let the amplitude of the two-way azimuth antenna pattern be $W_a(\phi)$, where ϕ represents the azimuth squint angle. To reduce computational complexity, let us assume the following simple conversion between frequency and azimuth angle.

$$f = \frac{2V_{st}}{\lambda}\phi.$$

The scalloping effect is compensated by multiplying the data by the inverse of

$$\hat{W}_a(k) = W_a\left[\frac{\lambda}{2V_{st}}\left(k - \frac{N_a}{2}\right)\frac{PRF}{N_a}\right],$$

where $0 \leq k \leq N_a - 1$. The number inside the brackets represents the azimuth off- foresight angle.

6.6 Geometric Rectification

Following the deramp FFT processing, the burst image is presented in the slant range-Doppler domain. For convenience, the azimuth pixels are rotated so that the Doppler centroid line always shows up at the center of the burst image. The geometric rectification algorithm is used to resample the burst image from the slant range-Doppler domain into the ground range along-track and cross-track domain ready for multi-look overlay.

The geometric rectification algorithm contains three major functions:

(a) Fanshape resampling: Resample the image from the range-Doppler domain into a rectangular grid format in the slant range domain;

(b) Image deskew (or rotation): Deskew the image into the along-track and cross-track directions in the slant range domain;

(c) Slant-to-ground range conversion: Convert the slant range image into the ground range domain.

In the following, we show that these three major functions can be accomplished by two one-dimensional resampling steps with the range resampling performed before the azimuth resampling. Let C_1 represent the distance in the along-track direction and C_2 the distance in the cross-track direction. The range resampling interpolates the intercept points of the "'ground range line" and the constant C_2 line. The azimuth resampling then interpolates the intercept points of the constant C_2 line and the constant C_1 line.

6.6.1 Range Resampling Algorithm

Let r_{sl} be the slant range measured from the center of the illumination burst, R_{en} the earth radius at nadir, R_{et} the earth radius at the center of swath, h the spacecraft altitude and Δr the desired output range pixel spacing.

Let us consider the ith range pixel in the kth range line, where $i \geq 0$ and $0 \leq k \leq N_a - 1$. To simplify the notation, we consider the case for a given range line, The slant range measured from the center of the illumination burst is

$$r_{sl}(i) = r_{sl}(0) + i\frac{c}{2f_s}s,$$

where s = 4 represents the range bandwidth reduction factor. Let us assume that the Doppler parameters are updated every I range pixels and there are M range blocks. Let the Doppler parameters of the mth block be represented by $f_d(m)$ and $f_r(m)$, where $0 \leq m \leq M-1$. The Doppler frequency of the ith range pixel in the kth range line is given by

$$f(i) = f_d(m) + \left(k - \frac{N_a}{2}\right)\frac{PRF}{N_a}.$$

The point of the closest approach to the flight track in the slant range domain is given by

$$R'_s(i) = r_{sl}(i) - \frac{\lambda}{4}\frac{[f(i)]^2}{|f_r(m)|}$$

and the point of the closest approach to the nadir track in the ground range domain is given by

$$R'_g(i) = R_{et}\cos^{-1}\frac{R_{et}^2 + (h + R_{en})^2 - (R'_s(i))^2}{2R_{et}(h + R_{en})},$$

where the corresponding output range pixel index is

$$i' = \frac{R'_g(i) - R'_{g0}}{A\,r} = h(i),$$

The term R'_{g0} represents the cross-track distance from the first output pixel to the nadir track and is pregenerated based on the maximum expected, Doppler frequency.

The same procedure is repeated at a number of locations across the swath. A polynomial (quadratic) function, g(.), is then used to relate the input and output indices by

$$i = g(i').$$

Note that functions g(.) and h(.) are range line dependent. Let

$$i'_{min} = h(0) \ .$$

Apply range rectification for output range pixels, $i' \geq i'_{min}$. After range rectification, corner turn the data into azimuth direction.

6.6.2 Azimuth **Resampling** Algorithm

Note that if the Doppler parameters are updated in the slant range domain using a constant update interval, I, the update block size in the ground range domain may be variable. For the mth range block, there are $I'(m)$ pixels, where

$$I'(m) = h[(m+1)I] - h[mI] .$$

Let V_{sw} represent the swath velocity, p the burst period in number of pulses, PBW the processing bandwidth and Ax the desired output azimuth pixel spacing. Let us consider the kth azimuth pixel in the mth range block. Use the processing Doppler parameters in azimuth rectification. "The Doppler frequency is

$$f(k) = f_d(m) + \left(k - \frac{N_a}{2}\right)\frac{PRF}{N_a}.$$

The maximum output azimuth pixel index of the nth burst image is

$$k'_{max}(m) = \frac{n\frac{p}{PRF}V_{sw} + \frac{f_d(m)+\frac{PBW}{2}}{|f_r(m)|}V_{sw}}{\Delta x}$$

and the minimum index is

$$k'_{min}(m) = \frac{n\frac{p}{PRF}V_{sw} + \frac{f_d(m)-\frac{PBW}{2}}{|f_r(m)|}V_{sw}}{\Delta x}.$$

The Doppler frequency is related to the output pixel index by

$$f(k') = \frac{k'\Delta x - n\frac{p}{PRF}V_{sw}}{V_{sw}}|f_r(m)|,$$

for $k'_{min}(m) \le k' \le k'_{max}(m)$ *and*

$$k = \frac{f(k') - f_d(m)}{\frac{PRF}{N_a}} + \frac{N_a}{2},$$

where $0 \le k \le N_a - 1$.

Apply azimuth rectification as specified by the above equations. After azimuth rectification, keep the data in the azimuth direction.

6.7 Multi-Look Overlay

Let

$$K'_{\min} = \min \{k'_{min}\}$$

and

$$K'_{\max} = \max\{k'_{max}\} .$$

Create a buffer for each geometric rectified burst image, where $K'_{\min} \le k' \le K'_{\max}$. Write the rectified burst image into this buffer as specified by the corresponding $k'_{min}(m)$ and $k'_{max}(m)$ indices. For each k', calculate the range shifts as follows.

$$f(k') = \frac{[k' - K'_{\min}]\Delta x}{V_{sw}} f_r(0)| + \left(f_d(0) - \frac{PBW}{2} \right) .$$

Substitute $f(k')$ and $r_{sl}(0)$ into the equations on page 55 to calculate the starting output range pixel. Let it be i'_{min}(k'). Write and add the k' range line of the azimuth shifted data into the multi-look overlay buffer starting from the $i'_{min}(k')$ range pixel,

Repeat the same procedure for each burst image. In addition, maintain a separate two-dimensional array as a look counter which counts the number of additions for each output pixel. After the burst images are overlaid, divide the image pixel value by the look counter on a pixel by pixel basis.

6.8 Doppler Centroid Estimation

For the SIR-C survey processor, the initial Doppler centroid frequency is estimated using the PRF scan data. This Doppler centroid frequency is then updated and tracked by a burst mode clutterlock algorithm throughout the survey processing.

6.8.1 Burst Mode Clutterlock Algorithm

The clutterlock algorithm is performed after the azimuth compression and before the along-track radiometric compensation. It utilizes the azimuth antenna pattern modulation characteristics of the burst images to estimate the Doppler centroid frequency. It consists of four major steps: a) Azimuth line intensity averaging; b) Energy balancing; c) Running average/linear-fit in azimuth; and d) Quadratic-fit in range.

First of all, the azimuth line data are energy detected and averaged every TBD lines to reduce the noise effects.

Secondly, each averaged azimuth line is divided into four equal portions centered at an azimuth pixel. Let the energy of each portion be denoted by El, E_2, E_3 and E_4 from left to right respectively. For each averaged line, the energy difference between the left-side and right-side of each azimuth pixel is calculated.

$$\Delta E = |E_1 + E_2 - E_3 - E_4| .$$

To ensure that the estimate converges to the centroid of the antenna pattern rather than the dip of the antenna pattern, it is checked that

$$E_2 + E_3 > E_1 + E_4 .$$

The azimuth pixel, $\hat{k}$, that minimizes the energy difference, ΔE, represents the new Doppler centroid estimate.

$$f_d = f_d + \left(\hat{k} - \frac{N_a}{2}\right)\frac{PRF}{N_a}$$

Thirdly, a running average in the azimuth direction is applied. The motivation of the running average is to estimate the Doppler centroid frequency based on a larger data set since a single burst image is too small to produce an accurate Doppler centroid estimate. For the

SIR-C survey processor, running average using TBD burst Doppler estimates is selected. Azimuth linear-fit is then applied to the running averaged Doppler centroid frequencies to take advantage of the linear Doppler drift characteristics. The azimuth linear-fit is applied to sixteen running averaged Doppler centroid frequencies.

Lastly, the range quadratic-fit is applied to the running averaged/azimuth linear-fit Doppler centroid frequencies.

6.8.2 **Quality Check**

The accuracy of the Doppler centroid estimates strongly depends on the Signal-to-Noise Ratio (SNR) of the data, which varies as a function of range distance, and the scene characteristics. It is necessary to reduce the effects caused by the small SNR and variable scene characteristics.

An SNR profile as a function of azimuth line index (range pixel index) is generated based on the SNR at the center of swath and the range antenna pattern compensation vector (including range antenna pattern, range attenuation and incidence angle). An SNR variation cut-off threshold is selected.

Besides, the ΔE divided by the sum of energies, expressed as a function of azimuth pixel index, is generated for each averaged azimuth line. The normalized ratio serves as the quality check indicator for each Doppler centroid estimate.

All the data are used in clutterlock (energy balancing), Two passes are employed as quality check routines. The first pass is performed in the azimuth running average: It only uses the Doppler estimates whose SNR and quality indicators are greater than the preset thresholds. The second pass is performed in the range quadratic fit: It only uses the Doppler estimates whose errors are less than TBD times the standard deviation. These quadratic fit parameters are then extrapolated to derive the estimates across the entire swath.

6.9 Doppler **Frequency Rate Determination**

In the SIR-C survey processor design, the overlap between the first (look-1) and fourth (look-4) burst images is far less than what is required to derive an accurate Doppler frequency rate estimate. The Doppler frequency rate will be determined from the ephemeris data and radar parameters. Analysis results show that the accuracy of the ephemeris data is sufficient for the survey processing.

The radar parameters, attitude vectors, position vectors, velocity vectors, orbit elements and DWP parameters are supplied by the Mission Operations Subsystem (MOS) during and post the mission. Since the position and velocity vectors are recorded in an one-minute interval, they are interpolated into a TBD time interval.

This approach is adopted as the baseline design. The header decode approach is reserved as a backup option in case the MCC orbit information is not available in time for the survey processing.

7. STANDARD PREPROCESSING ALGORITHM

The standard preprocessing algorithm include three major algorithms: clutterlock, autofocus and range cross-correlation algorithms. The clutterlock algorithm is used to estimate the Doppler centroid frequency. The autofocus algorithm is used to estimate the Doppler frequency rate. The range cross-correlation is used for the PRF ambiguity check. All three algorithms are designed to derive the estimates from the single-look full-aperture complex image data. To reduce the computational complexity, one quarter of the range chirp bandwidth is used in the range compression. The selection of the range processing spectrum is the same as that of the survey processing algorithm. The survey processing Doppler centroid estimates are used as the initial Doppler predicts.

Fig. 7.1 and Fig. 7.2 show the algorithm flowchart. Let N_a represent the azimuth FFT length used in the azimuth compression and K_a the number of range lines (azimuth pixels) used in the preprocessing. Following the 'No-point azimuth inverse FFT, only the first K_a pixels are retained for each azimuth line. Each azimuth line is transformed by K_a-point FFT to attain the frequency spectrum. At this point, the clutterlock, autofocus and range cross-correlation algorithms are applied to estimate the new Doppler parameters. These new Doppler parameters are used for the next azimuth compression iteration. The same procedure is iterated until the Doppler estimates converge.

The FFT length is selected as follows,

a) L-band: $N_a = 4$ K and $K_a = 1$ K;

b) C-band: $N_a = 2$ K and $K_a = 1$ K.

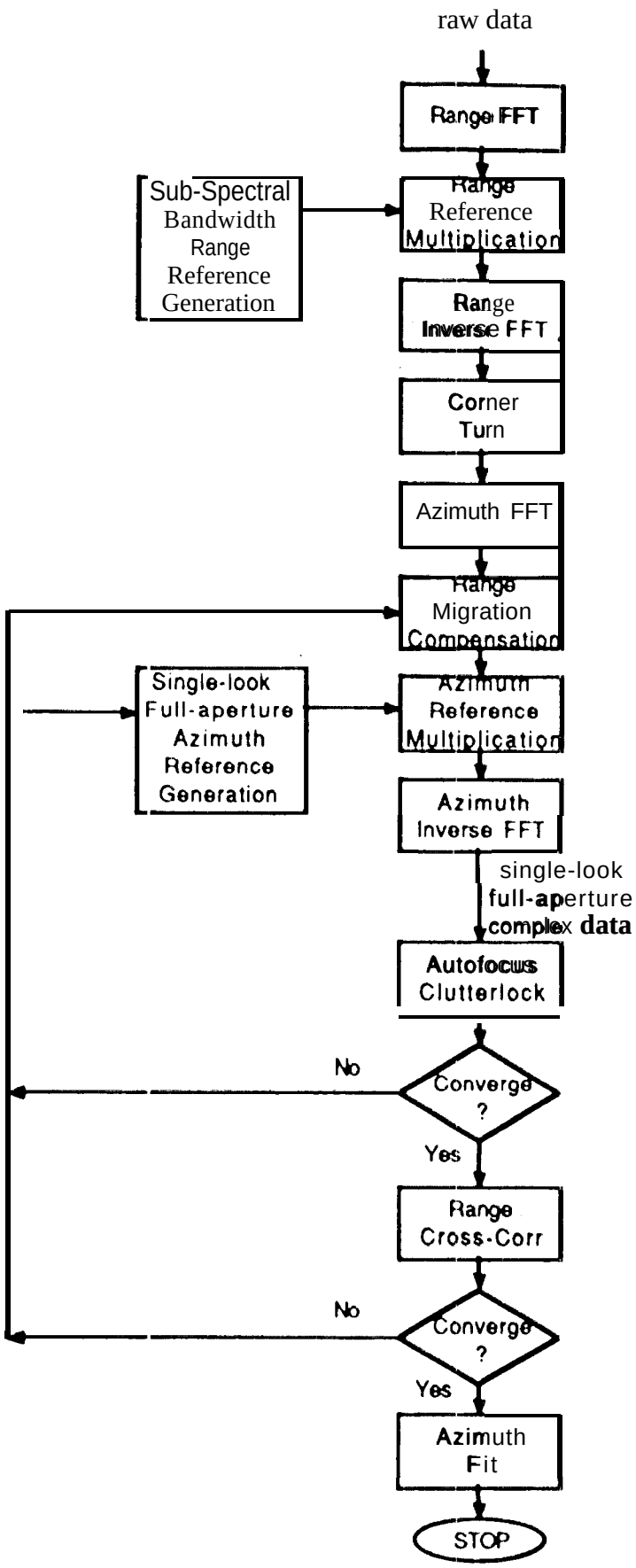

Fig, 7.1: Standard preprocessing algorithm flowchart,

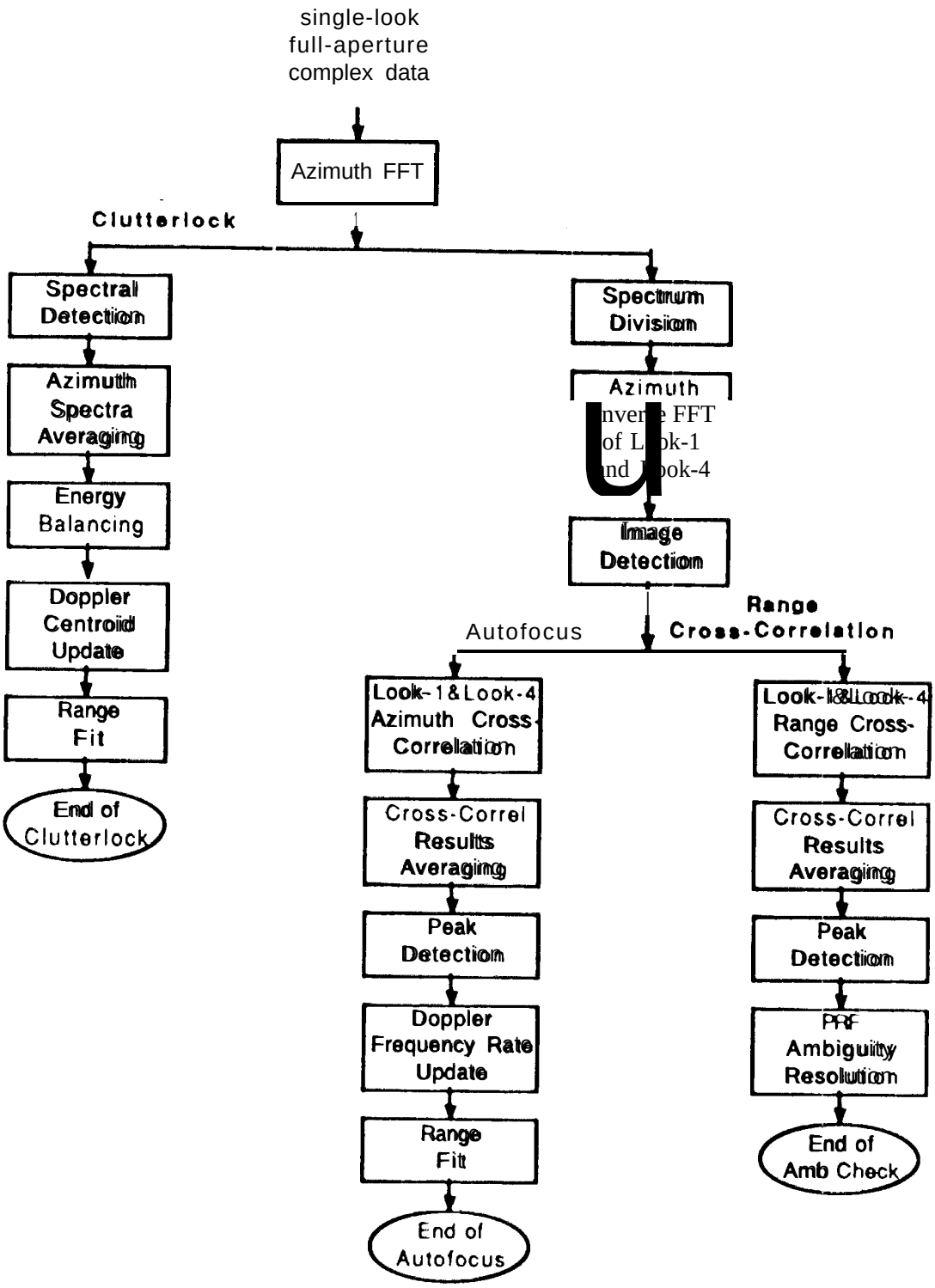

Fig. 7.2: Clutterlock, autofocus and range cross-correlation algorithm flowchart,

7.1 Doppler Centroid Estimation

For the clutterlock algorithm, the azimuth spectra are energy detected and averaged every $m_a (= 16)$ lines. The averaged spectra with a width equal to PBW are divided into four equal portions. Let the energy of each portion (look) be denoted by E_1, E_2, E_3 and E_4. from left to right respectively. For each averaged spectra, the energy difference between the left-side and the right-side of each frequency bin is calculated.

$$\Delta E = |E_1 + E_2 - E_3 - E_4| \, .$$

To ensure that the estimate converges to the centroid (peak) of the antenna pattern rather than the dip of the antenna pattern, it is checked that

$$E_2 + E_3 > E_1 + E_4 \, .$$

The frequency bin which minimizes the energy difference, ΔE, represents the new Doppler centroid estimate. Let

$$f_d = nPRF + \hat{f}_d,$$

where $0 \leq \hat{f}_d < PRF$. Also let

$$\hat{k} = \mathrm{rnd}\left\{ \frac{\hat{f}_d}{PRF} N_a \right\},$$

where rnd(.) represents the round-off operation and $\hat{k}$ represents the frequency bin of the processing Doppler centroid frequency. Let $\tilde{k}$ be the frequency bin of the new Doppler centroid estimate. If $\tilde{k} \geq \frac{N_a}{2}$, then the new Doppler centroid frequency in terms of Hz is

$$f_d = \begin{cases} \tilde{k}\frac{PRF}{N_a} + (n+1)PRF, & \text{for } 0 \leq \tilde{k} \leq \hat{k} - \frac{N_a}{2} - 1. \\ \tilde{k}\frac{PRF}{N_a} + nPRF, & \text{for } \hat{k} - \frac{N_a}{2} \leq \tilde{k} \leq N_a - 1; \end{cases}$$

If $\tilde{k} < \frac{N_a}{2}$, then

$$f_d = \begin{cases} \tilde{k}\frac{PRF}{N_a} + nPRF, & \text{for } 0 \leq \tilde{k} \leq \hat{k} + \frac{N_a}{2} - 1; \\ \tilde{k}\frac{PRF}{N_a} + (n-1)PRF, & \text{for } \hat{k} + \frac{N_a}{2} \leq \tilde{k} \leq N_a - 1. \end{cases}$$

These new Doppler centroid estimates are then quadratic fit across the swath.

7.2 **Doppler Frequency Rate Estimation**

The azimuth spectra centered at the Doppler centroid frequency with a width equal to PBW are divided into four equal portions. Each portion corresponds to one look. The look-l and look-4 spectra are transformed by \$-point inverse FFT to obtain the single-look complex images. The complex image data are magnitude detected.

For the autofocus algorithm, the detected look-l and look-4 image data are azimuth cross-correlated for each azimuth line. The cross-correlation is done as follows: a) FFT look-1 and look--l magnitude detected data ($\frac{K_a}{4}$-point real FFT); b) Complex conjugate multiply these two spectra (look] $\times$look4*); c) Oversample the data by basebanding and zero padding the center of the spectra; and d) inverse FFT the zero-padded spectra ($nK_a/4$-point inverse complex FFT), where n represents the oversampling factor. For the SIR-C, $n = S$ and $K_a/4 = 256$. The cross-correlation results are averaged across the range. The peak locations of the averaged azimuth cross-correlation results are translated into new Doppler frequency rate estimates as follows.

$$f_r = f_r + \Delta f_r ,$$

where

$$\Delta f_r = \frac{16}{3} \frac{|f_r|}{T\ PRF} \Delta x$$

and $f_r < 0$. The term Ax in the unit of azimuth pixels (including a factor of four caused by look image generation; excluding the oversampling factor) represents the peak location of the cross-correlation results. When Ax > 0, it means these two image looks are too close to each other. The $|f_r|$ value has to be decreased, or equivalently bringing these two image looks farther apart. The Doppler frequency rate estimates are then quadratic fit across the swath.

7.3 **Range Cross-Correlation**

For the range cross-correlation, the magnitude detected data of the look-1 and look-4 images are range cross-correlated. The cross-correlation results are averaged in azimuth. The peak location of the averaged range cross-correlation results is translated into the PRF ambiguity number.

$$\hat{n} = \frac{4}{3}\frac{\frac{s\,c}{f_s}}{\lambda T\, PRF}\Delta r \ ,$$

where s = 4 for the SIR-C, representing the range bandwidth reduction (or presuming) factor. The term Δr in the unit of range pixels represents the peak location of the cross-correlation results. It is defined to be the range offset of look-4 image relative to look-1 image. When Δr >0, it means the look-4 image is sitting too close to the flight track. To bring it to be at the same range as the look-l image, the processing Doppler centroid has to be increased. Thus, the true Doppler should be

$$f_d = f_d + \hat{n} PRF.$$

This range cross-correlation approach is only used for PRF ambiguity check. It is not intended to be used for PRF ambiguity resolution.

7.4 Quality Check

The accuracy of the Doppler estimates strongly depends on the Signal-to-Noise Ratio (SNR) of the data, which varies as a function of range distance and the scene characteristics. To remove the effects caused by the small SNR, an SNR profile as a function of azimuth line index (range pixel index) is generated based on the SNR at the center of swath (derived by the quality assurance algorithm) and the range antenna pattern compensation vector (including range antenna pattern, range attenuation and incidence angle). An SNR variation cut-off threshold is selected.

in the clutterlock algorithm, the ΔE divided by the sum of energies, expressed as a function of frequency bin, is generated for each averaged spectra, The normalized ratio serves as the quality indicator for each Doppler centroid estimate, Similarly, in the autofocus algorithm, the cross-correlation function is generated for each azimuth line. The peak-to-mean ratio is used as the quality indicator for each Doppler frequency rate estimate.

All the data are used in clutterlock (energy balancing) and autofocus (look cross-correlation). Two passes are employed in the quadratic fit as quality check routines. The first pass applies the quadratic fit to the Doppler estimates whose SNR and quality indicators are greater than the preset thresholds. This quadratic fit also produces a goodness of fit, the standard deviation. The second pass excludes the outliers in the quadratic fit, i.e., only the Doppler estimates whose errors are less than TBD times the standard deviation are used. These quadratic fit parameters are then extrapolated to derive the estimates across the entire swath.

7.5 **Two-Dimensional Doppler Fit**

The number of locations selected for the preprocessing is as follows: For both L-band and C-band. three locations for the Multi-Look Image Product and two locations for the Single-Look Image Product are applied in preprocessing.

These Doppler parameter estimates (including all three coefficients: near range Doppler, linear slope and quadratic component) are then gone through a quadratic fit in the along track direction. The coefficients of the polynomial fit are then used to generate the Doppler parameters for each processing block during the standard data processing.

8. STANDARD PROCESSING ALGORITHM

The range Doppler processing algorithm with secondary range compression is selected as the SIR-C standard processing algorithm. It is a continuous mode SAR processing algorithm. For fast computation, the range compression and azimuth compression are performed in the frequency domain using FFT. The single-look full-aperture approach is adopted as the azimuth compression algorithm. The azimuth compressed data are azimuth deskewed to fern] the azimuth deskewed single-look complex image from which the multi-look image is generated. The algorithm flowchart is shown in **Fig. 8.1.**

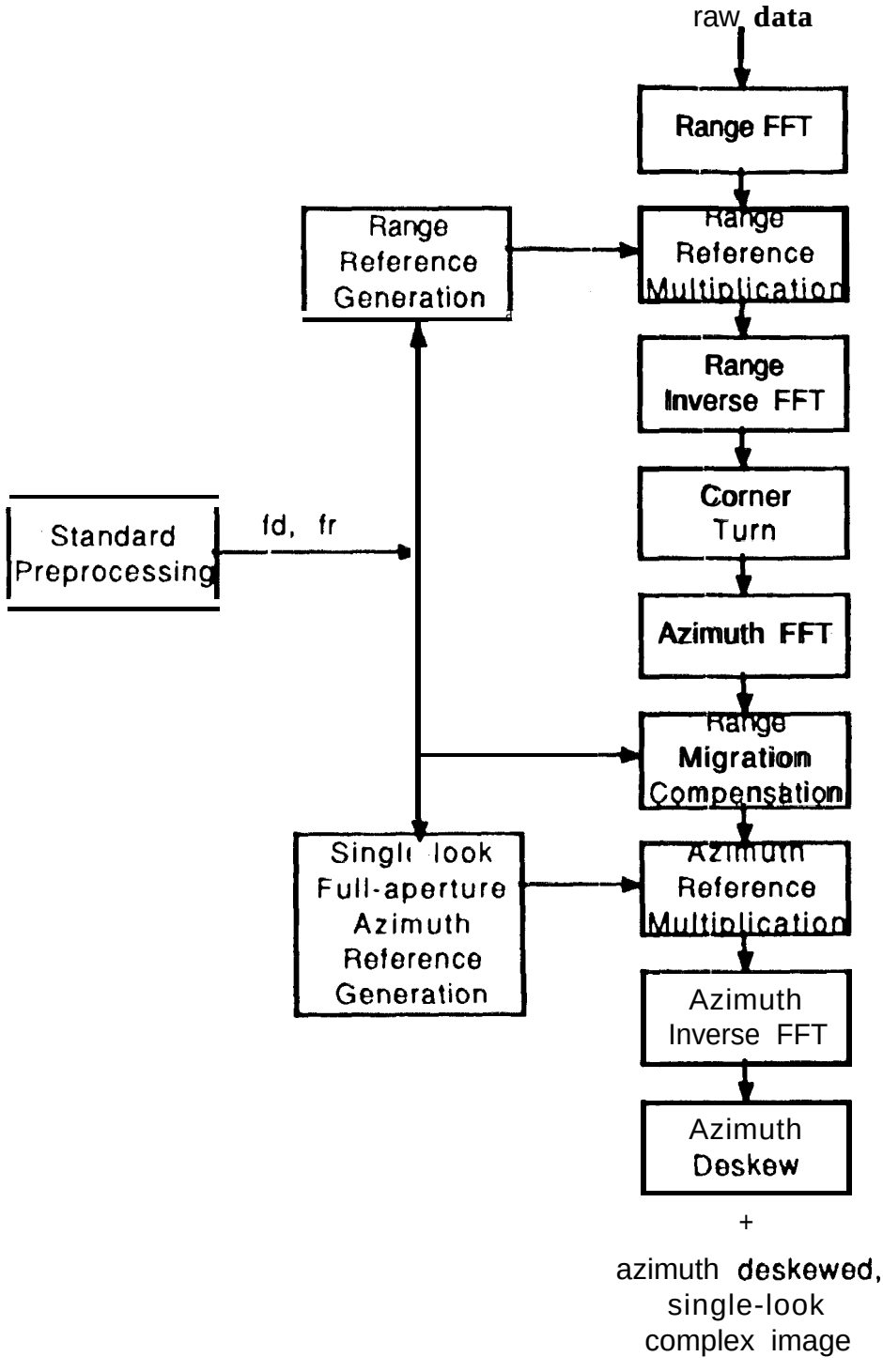

Fig. 8.1: Standard processing algorithm flowchart.

Let us use the following notations:

$h(r)$: range reference function;

h(r): azimuth reference function;

f_d: Doppler centroid frequency;

f_r: Doppler frequency rate, f_r < O;

PBW: azimuth processing bandwidth;

7': full synthetic aperture time;

$R(f)$: range migration equation in the frequency domain;

f_s: range complex sampling rate;

B: range chirp bandwidth;

τ: range chirp pulse duration;

b_0: range chirp rate without secondary range compression;

b_1: range chirp rate of secondary range compression;

6: range chirp rate with secondary range compression;

f_0: range chirp start frequency;

c: speed of light;

λ: wavelength;

L_a: azimuth reference function length;

L_r: range reference function length;

N_a: azimuth FFT length;

N_r: range FFT length;

N_r^o: number of complex range samples;

V_{sw}: swath velocity;

θ_I: incidence angle;

r_{sl}: near range slant range.

8.1 Range Compression

8.1.1 Range Reference Function

The range reference function is generated in the time domain. To accommodate large range walk, the secondary' range compression is employed to compress the range dispersed point-target response. This results in a Doppler dependent range reference function. Since the Doppler drifts in the along-track direction, the range reference function must be updated accordingly. For simplicity, the range reference function is updated every processing block for both I,-band and C-band. There is no update of range reference function required in the cross-track direction.

The range reference function is generated as follows.

$$
\begin{aligned}
H(f) &= \mathcal{F}\{h(r)\} \\
h(r) &= e^{j\phi(r)} \\
\phi(r) &= 2\pi\left[f_0 \frac{(r' - \tau_r)}{f_s} + \frac{1}{2} b \left(\frac{(r - \tau r)}{f_s} \right)^2 \right],
\end{aligned}
$$

for $0 \leq r \leq L_r - 1$, where τ_r represents the range time delay included to account for registration error among multiple channel data, and

$$
\begin{aligned}
L_r &= \tau f_s \\
b_0 &= \pm \frac{B}{\tau} \\
b_1 &= - f_r \left(\frac{c}{\lambda f_d} \right)^2 \\
b &= b_0 \left(\frac{1}{1 + \frac{b_0}{b_1}} \right) \\
f_0 &= \frac{f_s \mp B}{2}
\end{aligned}
$$

for the up-chirp and down-chirp respectively. The SIR-C uses the down-chirp.

The cosine squared plus pedestal function is selected as the weighting function to control the sidelobe ratios. The pedestal height is selected to be 0.45. The weighting function is generated and multiplied with the reference function in the time domain.

$$
w(r) = (1 - H) \left[\cos^2 \frac{\pi \left(r - \frac{L_r}{2} \right)}{L_r} \right] + H .
$$

where $0 \leq H \leq 1$ and $0 \leq r \leq L_r - 1$.

8.1.2 Range Compression

The range compression is accomplished in four steps:

(a) Range FFT the raw signal data;

(b) Complex conjugate multiply the signal spectrum with the reference function spectrum ($X(f)H^*(f)$). Since the SIR-C signal data is real, only the first half of the spectrum is multiplied with the reference function;

(c) Baseband shift; and

(d) Inverse range FFT.

Following the range compression, the last L_r range pixels in the time domain are discarded. This leaves $N_r^o - L_r$ good range compressed pixels.

The memory size is selected such that both the I,-band data and the C-band data can be processed in full subswath. The range FFT length is selected as follows:

(a) Single-polarization: forward FFT:16 K real, inverse FFT: 8 K complex;

(b) Dual-polarization: forward FFT:8 K real, inverse FFT: 4 K complex;

(c) Quad-polarization: forward FFT:4 K real, inverse FFT:2 K complex.

8.2 **Azimuth Compensation**

The single-look full-aperture azimuth compression algorithm is selected. It is accomplished in four major processing steps:

(a) Azimuth FFT the range compressed data:

(b) Range migration compensation in the range-Doppler domain;

(c) Complex conjugate multiply the signal spectrum with the reference function spectrum $(X(f)H^*(f))$; and

(d) Azimuth inverse FFT.

Following the azimuth inverse FFT, the last L_a azimuth pixels in the time domain are discarded.

The azimuth FFT length is selected as follows:

(a) L-band: 4 K complex;

(b) C-band: 1 K complex.

Detailed processing steps are described in the following subsections,

8.2.1 **Frequency Bin Definition**

Let us use the following notations:
f_d: unambiguous Doppler centroid frequency;
$\hat{f}_d$: ambiguous Doppler centroid frequency, where $0 \le \hat{f}_d < PRF$;
$f(j)$: frequency bin, where $0 \le j \le N_a - 1$;
n: PRF ambiguity number.

The frequency value of each frequency bin is assigned as follows. Let

$$n = \text{int}\left\{\frac{f_d}{PRF}\right\}$$

and

$$\hat{f}_d = f_d - nPRF,$$

where $\mathrm{int}(x)$ represents the maximum integer that is less than or equal to x. Also let

$$\hat{j} = \mathrm{rnd}\left\{\frac{\hat{f}_d}{PRF} N_a\right\},$$

where rnd(.) represents the round-off operation and $\hat{j}$ represents the frequency bin of the Doppler centroid frequency. If $\hat{j} \geq \frac{N_a}{2}$, then

$$f(j) = \begin{cases} j\frac{PRF}{N_a} + (n+1)PRF, & \text{for } 0 \leq j \leq \hat{j} - \frac{N_a}{2} - 1. \\ j\frac{PRF}{N_a} + nPRF, & \text{for } \hat{j} - \frac{N_a}{2} \leq j \leq N_a - 1; \end{cases}$$

If $\hat{j} < \frac{N_a}{2}$, then

$$f(j) = \begin{cases} j\frac{PRF}{N_a} + nPRF, & \text{for } 0 \leq j \leq \hat{j} + \frac{N_a}{2} - 1; \\ j\frac{PRF}{N_a} + (n-1)PRF, & \text{for } \hat{j} + \frac{N_a}{2} \leq j \leq N_a - 1. \end{cases}$$

8.2.2 **First and Last Output Azimuth Lines**

Notations:

r: first output azimuth line;

.s:]ast output azimuth line;

N_r: number of range samples or number of azimuth lines;

i: range sample index or azimuth line index, where O $\leq$ i $\leq N_r - 1$;

$t_{min}(i)$: time since Doppler centroid that gives the minimum range migration;

t_{max} (i): time since Doppler centroid that gives the maximum range migration;

$f_d(i)$: Doppler centroid of the ith azimuth line;

$f_r(i)$: Doppler frequency rate of the ith azimuth line, where $f_r(i) <$ O;

$L_a(i)$: azimuth reference function length of the ith azimuth line; and

$/_1$: interpolator length used in the range migration compensation.

For each azimuth line, calculate

$$t_{min}(i) = \begin{cases} -\frac{f_d(i)}{f_r(i)}, & \text{if } |f_d(i)| < \frac{PRF}{2}; \\ +\frac{PRF}{2f_r(i)}, & \text{if } f_d(i) \leq -\frac{PRF}{2}; \\ -\frac{PRF}{2f_r(i)}, & \text{if } f_d(i) \geq \frac{PRF}{2}; \end{cases}$$

and

$$t_{max}(i) = \begin{cases} -\frac{PRF}{2f_r(i_r(i))}, & \text{if } f_d(i) < 0; \\ +\frac{PRF}{2f_r(i)}, & \text{if } f_d(i) \geq 0. \end{cases}$$

Then, r is the minimum number of i such that

$$\frac{\lambda}{c/f_s}\left[f_d(i)t_{min} + \frac{1}{2}f_r(i)t_{min}^2\right] + i \geq \frac{l_1}{2} - 1.$$

and s is the maximum number of i such that

$$\frac{\lambda}{c/f_s}\left[f_d(i)t_{max} + \frac{1}{2}f_r(i)t_{max}^2\right] + i < N_r - \frac{l_1}{2}.$$

8.2.3 **Azimuth FFT**

Take FFT of all the azimuth lines,

8.2.4 **Range Migration indices Generation**

'1'0 facilitate the vector processing functions to improve the efficient usage of the computational elements, the range migration compensation is performed in the range dimension. The data is corner-turned following the azimuth FFT for fast data access in the range direction. Following the range migration compensation, the data is corner-turned back into the azimuth direction such that the azimuth reference function multiplication and the azimuth inverse FFT can be applied efficiently.

Notations:

j: frequency bin index, where O $\leq$ j $\leq N_a - 1$;

d(j): range migration indices;

$u(j)$: index vector;

$v(j)$: fraction vector; and

f (i, j): the frequency value of the ith range sample of the jth range line.

The frequency value is determined by the procedure presented in Section 8.2,1. The range

migration indices are then generated as follows.

$$t(i, j) = \frac{f(i, j) - f_d(i)}{f_r(i)}$$

$$d(i, j) = \frac{\lambda}{c/f_s}\left[f_d(i)t(i, j) + \frac{1}{2}f_r(i)t^2(i, j)\right] + i$$

$$u(i, j) = \text{int}\ \{d(i, j)\}$$

$$v(i, j) = d(i, j) - \text{int}\ \{d(i, j)\}$$

8.2.5 **Range Migration Compensation**

The fraction vector, $v(i, j)$, is then used to look up the pregenerated interpolation coefficients table. Four interpolation coefficient vectors are generated accordingly.

The interpolation coefficients are pregenerated as follows. Let them be expressed by " l-points n-bins". The parameter " l-points" represents the length of the interpolator, i.e., the number of data points used in the interpolation. The parameter "n-bins" represents the number of bins divided between two adjacent data points, which is used to interpolate the data between two adjacent data points.

Let w(.) be the interpolation function and x_i be the data points.

$$x_{i+d} = \sum_{k=-\frac{l}{2}+1}^{\frac{l}{2}} x_{i+k}w(k - d),$$

where d, representing a fraction of a bin, is quantized into an $1/n$ step size, ranging from O to $(n-1)/n$. For the SIR-C processor, the cubic spline interpolator is selected and $l = 4$ and $n = 32$, i.e., a 4-point interpolator with 32 bins is used for the range migration compensation.

The index vector, u(i, j), is then used to access the data along the range migration curve. Four data vectors are generated accordingly.

The interpolation is done by multiplying the data vectors with the interpolation vectors and summing up the multiplication results.

8.2.6 Azimuth Reference Function Generation

The azimuth reference function is generated in the time domain. Since there is severe Doppler drift in both along-track and cross-track directions, the azimuth reference function must be updated accordingly. The azimuth reference function is updated every processing block in the along-track direction. In the cross-track direction, it is updated according to the update rate. The azimuth reference function length is variable as a function of range to attain a constant resolution. To simplify the registration between the H- and V-channel image, the average of the Doppler estimates is used as the processing Doppler frequency.

$$L_{max} = \max_{0 \le i \le N_r - 1} \{L_a(i)\} = L_a(N_r - 1).$$

The azimuth reference function is generated as follows.

For the SIR-C, the transmitted pulses of V and H polarizations are interleaved and offset by exactly half of the interpulse period. Targets from the set of HH and HV and the set of VH and VV data are offset in the along-track direction by a half of a azimuth pixel. To eliminate this constant offset such that the multi-polarization image data arc registered, two sets of azimuth reference functions are generated. For the HH and HV polarizations,

$$H(f) = \mathcal{F}\{h(x)\}$$
$$h(x) = e^{j\phi(x)}$$
$$\phi(x) = 2\pi \left\{ f_d \left(x - \frac{L_{max}}{2} \right) \frac{1}{PRF} + \frac{1}{2} f_r \left[\left(x - \frac{L_{max}}{2} \right) \frac{1}{PRF} \right]^2 \right\},$$

and for the VH and VV polarizations,

$$H(f) = \mathcal{F}\{h(x)\}$$
$$h(x) = e^{j\phi(x)}$$
$$\phi(x) = 2\pi \left\{ f_d \left((x \pm 0.5) - \frac{L_{max}}{2} \right) \frac{1}{PRF} + \frac{1}{2} f_r \left[\left((x \pm 0.5) - \frac{L_{max}}{2} \right) \frac{1}{PRF_1} \right]^2 \right\},$$

where $0 \le x \le L_a - 1$.

$$L_a(i) = \frac{PBW}{|f_r(i)|} PRF.$$

The " –" is used when the V channel is returned in the first half, between V transmit and H transmit. Conversely, the "+" is used when the V channel is returned in the second half, between H transmit and V transmit.

Again, the cosine squared plus pedestal function is selected as the window function to control the sidelobe ratios. The pedestal height is selected to be 0.45. The weighting function is generated and multiplied with the reference function in the time domain. The azimuth reference function is then FFT'ed.

8.2.7 Reference Function Multiplication

Complex conjugate multiply the range migration compensated, azimuth spectral lines with the spectra of the azimuth reference functions $(X(f)H^*(f))$.

8.2.8 Inverse Azimuth FFT

Take inverse azimuth FFT of the multiplied spectra and rotate the spectra to baseband.

8.3 **Azimuth Deskew**

The, processing Doppler parameters are updated in the along-track direction to accommodate the attitude drift. This along-track Doppler update causes significant relative skew and azimuth offset among image blocks. For some cases, the skew can be greater than the image block size, which 'is particularly true for the C-band. It also creates non-negligible range offset which must be compensated. The image data thus must be resampled before being merged into a long strip image.

Let us use the following notations:

n: azimuth block index, $0 \le n \le M_a - 1$;
M_a: number of azimuth blocks;
i: azimuth line index, $O \le i \le N_r^o - L_r - 1 = N_r - 1$;
$f_d^{[n]}(i)$: Doppler centroid frequency of the ith azimuth line in the nth azimuth block;
$f_r^{[n]}(i)$: Doppler frequency rate of the ith azimuth line in the nth azimuth block, $f_r < O$;
$x_{skew}^{[n]}(i)$: resampling index of the ith azimuth line in the nth azimuth block;
$x_{global}(i)$: resampling index of the ith azimuth line in the 0th azimuth block;
$x_{relative}^{[n]}(i)$: resampling index of the relative skew between the nth and Oth azimuth blocks:
$x_{start}^{[n]}$: start range line index of the nth azimuth block;
$d^{[n]}(i)$: fractional part of the resampling index of the ith azimuth line in the nth azimuth block;
$I_{read}^{[0]}(i)$: memory read index of the ith azimuth line in the Oth azimuth block;
$I_{write}^{[n]}(i)$: memory write index of the ith azimuth line in the nth azimuth block.

The proposed azimuth deskew algorithm is described as follows. The resampling indices of a given image block are generated based on its azimuth skew, $x_{skew}^{[n]}(i)$. The azimuth skew is then expressed as the summation of the relative skew, $x_{relative}^{[n]}(i)$, and the skew of the reference block, $x_{global}(i)$. The resampling indices are decomposed into one fractional part, $d^{[n]}(i)$, **and** two integer parts: $I_{read}^{[n]}(i)$ and $I_{write}^{[n]}(i)$. The fractional part is used in the interpolation. After the interpolation, the offset among image blocks will only contain integer pixel shift. The term, $I_{write}^{[n]}(i)$, is used in the memory write. After the memory write in the azimuth dimension, the image blocks will be parallel to each other so that they can be merged into a long image strip. During the memory read in the range dimension, the data is read out along the path specified by the term, $I_{read}^{[n]}(i)$. This completes the azimuth deskew algorithm.

8.3.1 Resampling Indices Generation

The resampling indices are generated as follows.

$$
\begin{aligned}
& x_{skew}^{[n]}(i) + x_{start}^{[n]} \\
&= \left(\left[\frac{f_d^{[n]}(i)}{f_r^{[n]}(i)} - \frac{f_d^{[o]}(0)}{f_r^{[o]}(0)} \right] \right) PRF \\
&+ x_{start}^{[n]} \\
&= \left(\left[\frac{f_d^{[o]}(i)}{f_r^{[o]}(i)} - \frac{f_d^{[o]}(0)}{f_r^{[o]}(0)} \right] \right) PRF \\
&+ \left(\left[\frac{f_d^{[n]}(i)}{f_r^{[n]}(i)} - \frac{f_d^{[o]}(i)}{f_r^{[o]}(i)} \right] \right) PRF \\
&+ x_{start}^{[n]} \\
&= x_{global}(i) + x_{relative}^{[n]}(i) + x_{start}^{[n]},
\end{aligned}
$$

where $f_r < 0$. The first term represents the skew of the reference azimuth block. The second term represents the relative skew between the nth and the reference azimuth block. The last term represents the start range line index of the nth azimuth block, Note that the memory write has the same direction as deskewing the data while the memory read has the opposite direction. Let

$$
\begin{aligned}
d^{[n]}(i) &= \text{frac}\left[x_{global}(i) + x_{relative}^{[n]}(i) \right] \geq 0 \\
I_{read}^{[n]}(i) &= \text{int}\left[x_{global}(i) \right] \\
I_{write}^{[n]}(i) &= x_{start}^{[n]}(i) - \text{int}\left[x_{global}(i) + x_{relative}^{[n]}(i) - d^{[n]}(i) - I_{read}^{[o]}(i) \right]
\end{aligned}
$$

The reference block is selected to be the one whose Doppler centroid is the average of the maximum and the minimum Doppler centroids. The advantage is the reduction in the relative skew amount,

8.3.2 Azimuth Interpolation

The fractional part, $d^{[n]}(i)$, is used to interpolate the ith azimuth line in the nth azimuth block. The interpolation is achieved by including a time delay in the time domain azimuth

reference function,

$$H(f) = \mathcal{F}\{h(x)\}$$
$$h(x) = e^{j\phi(x)}$$
$$\phi(x) = 2\pi \left\{ f_d \left(x - d^{[n]}\left(i - \frac{L_{mar}}{2}\right) \frac{1}{PRF} + \frac{1}{2} f_r \left[\left(x - d^{[n]}\left(i - \frac{L_{mar}}{2}\right) \frac{1}{PRF} \right)^2 \right] \right\},$$

for $0 \leq x \leq L_a - 1$.

8.3.3 Memory Write

Each interpolated azimuth line is written into the memory from $I^{[n]}_{write}(i)$ for a length of N_a -- 1,0 pixels.

8.3.4 **Memory Read**

The data is read out of the memory in the range dimension following the path specified by $I^{[o]}_{read}(i)$, i.e., the jth output range line is composed of

$$\left[I^{[o]}_{read}(i) + j \right],$$

for j $\geq$ O.

8.3.5 Range Offset Compensation

The range offset between the nth block and the reference block is

$$\Delta r^{[n]} = \frac{\lambda |f_d^{[o]}(0)|^2}{4 |f_r^{[o]}(0)|} - \frac{\lambda |f_d^{[n]}(0)|^2}{4 |f_r^{[n]}(0)|}.$$

When $\Delta r^{[n]} < 0$, it means block n should be placed closer to the flight track. Otherwise, it should be placed farther away from the flight track. This range offset information is compensated by including a time delay in the time domain range reference function.

$$H(f) = \mathcal{F}\{h(r)\}$$
$$h(r) = e^{j\phi(r)}$$
$$\phi(r) = 2\pi \left[f_0 \frac{r - \Delta r^{[n]}}{f_s} + \frac{1}{2} b \left(\frac{r - \Delta r^{[n]}}{f_s} \right)^2 \right],$$

8.4 Multi-Frequency Band **Data Processing**

'l'his section presents a design for registration of L-band and C-band images without extra resampling of data, It is assumed that registration is only permitted for the data acquired by the same PRF. Let us use the following notations:

t: start MET time converted from the start GMT time requested by the user;

s: start MET time of the image data produced by the processor;

τ: synthetic aperture time;

n: start processing line number;

f_d: reference Doppler centroid frequency;

f_r: reference Doppler frequency rate;

u: reference skew time;

V_{sw}: swath velocity;

Δx: pixel spacing,

The MET time of the first output image range line is the only parameter that is required for registration. It can be expressed as a function of the start data transfer time, the first processing range line number, the synthetic aperture time and the reference skew time as illustrated in Figure 1. This parameter will be saved in the CAS. We have

$$s^{[L]} = t^{[L]} + \frac{(n^{[L]} - 1)}{PRF} + \frac{\tau^{[L]}}{2} + u^{[L]}$$
$$s^{[C]} = t^{[C]} + \frac{(n^{[C]} - 1)}{PRF} + \frac{\tau^{[C]}}{2} + u^{[C]}$$

for L-band and C-band, respectively, where

$$u^{[L]} = \frac{f_d^{[L]}}{|f_r^{[L]}|}$$
$$u^{[c]} = \frac{f_d^{[C]}}{|f_r^{[C]}|}$$

are selected to be a multiple of $1/PRF$. If antenna beams are aligned, or equivalently the processing Doppler parameter is inversely proportional to the wavelength, then $u^{[L]} = u^{[C]}$.

Since t is in seconds and u is selected to be a multiple of $1/PRF$, if the synthetic aperture length is selected to be an even number, s PRF is in number of pulses (pixels). It implies that the I.-band and C-band single-look images will be automatically registered in the overlap region without extra data resampling. In the following, we discuss the registration for the multi-look images,

8,4.1 Simultaneous L-Band and C-Band Data Processing

If processing of L-band and C-band data is requested at the same time, it is designed such that the output image data will be registered starting from the first image range line.

The DTS will forward the tape until the MET time is equal to t. The L-band and C-band data (one at a time) will be transferred from the same start range line. Registration of the L-band and C-band images is controlled by selecting the start processing lines so that no extra resampling of the output data is required, The start processing lines, $n^{[L]}$ and $n^{[C]}$, are selected to be

$$n^{[L]} = 1$$
$$n^{[C]} = \left(\frac{\tau^{[L]} - \tau^{[C]}}{2} + u^{[L]} - u^{[C]} \right) PRF + 1$$

By doing so, the single-look images will be registered from the first output image line, so do the multi-look images. In the nominal condition, the difference in skew time is smaller than the difference in synthetic aperture time so that $n^{[C]} \geq 1$.

8.4.2 Non-Simultaneous L-Band and C-Band Data Processing

If processing of L-band and C-band data is requested at different time, it is designed such that the images will be registered in the overlap region.

The user has the options to register the new image with one of the previously processed images. The CAS will search for previously processed images that have overlap region with the new image and prompt the user to select one for registration. After the image is selected. the CAS will search for the image start MET time. Let it be s^o.

Again, registration is achieved by controlling the start processing line. The start processing

range line is the minimum n that satisfies

$$\left| \text{frac} \left\{ \frac{(s - s^o)V_{sw}}{\Delta x} \right\} \right| < \frac{1}{16} .$$

Note that the single-look images will be automatically registered in the overlap region. However, since the pixel spacing is changed for the multi-look images, they may not be registered. The idea of the above condition is select the start processing range line so that the registration error in the output images is less than one-sixteenth of an output pixel.

9. STANDARD POSTPROCESSING ALGORITHM

The standard postprocessing algorithm is used to generate the standard single-look image product, the standard multi-look detected image product and the standard multi-look complex image product- "from the azimuth deskewed single-look complex image data generated by the standard processor. The major function of the standard postprocessing algorithm include the cross-product generation, multi-look filtering and data reduction. The multi-look filtering combines the generation of multi-look imagery as well as the geometric rectification. The algorithm flowchart is shown in **Fig.** 9. 1

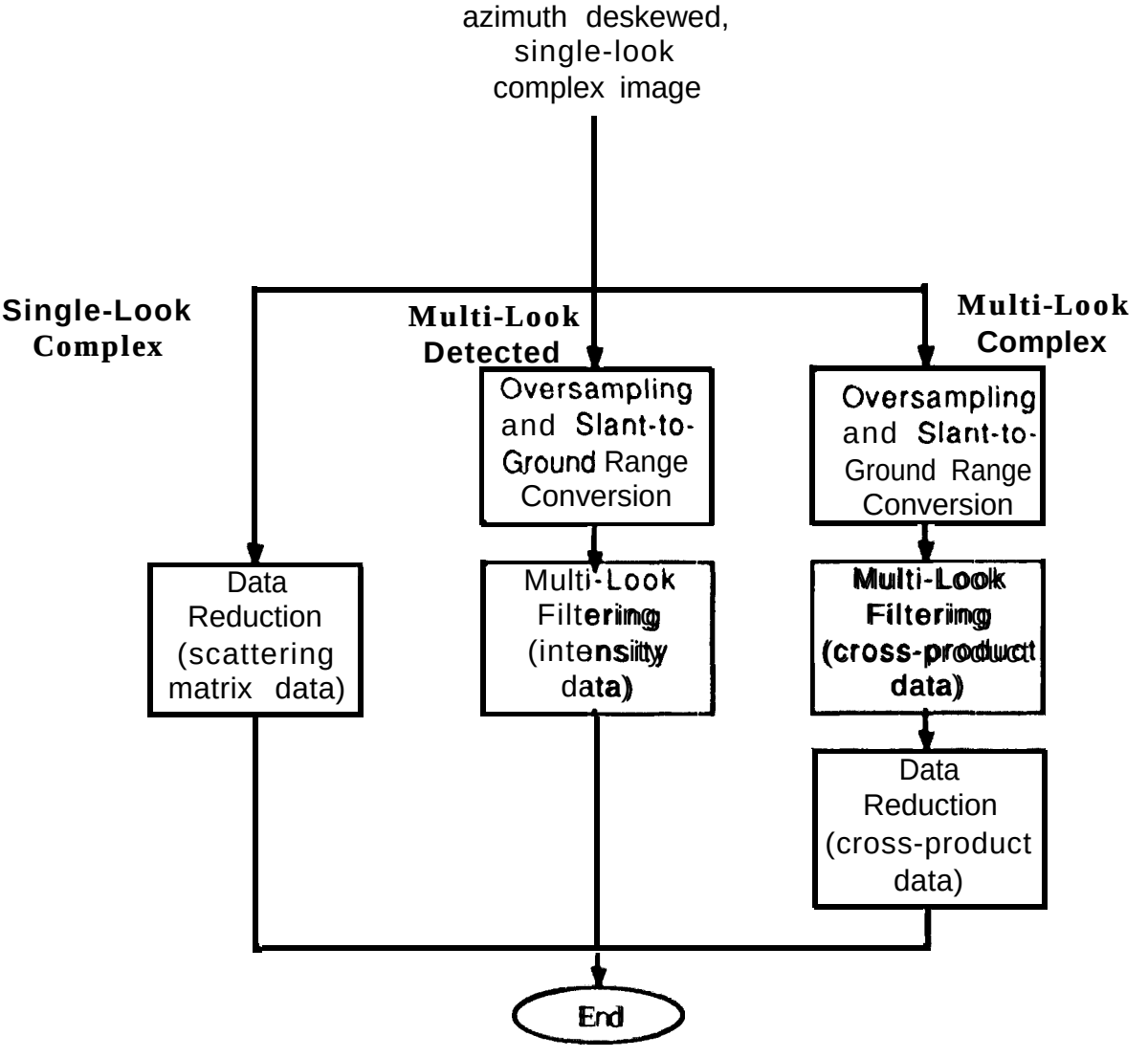

Fig. 9.1: Standard postprocessing algorithm flowchart.

9.1 Multi-Look Filtering

The multi-look filtering algorithm is employed to generate ground range, uniform resolution, equally spaced and speckly reduced multi-look image products by combining together the geometric resampling and low-pass filtering. For the SIR-C, it is proposed that all the high bandwidth (20 MHz) mode images and low bandwidth mode (10 MHz) images be filtered to a 25 m resolution in azimuth and a '25 m or natural resolution in range, The pixel spacing is selected to be 12.5 m in' both range and azimuth. For the single-polarization data, the filtering is applied to the intensity image. For the dual-polarization and quad-polarization data, the filtering is applied to the cross-products. To reduce the undersampling effect in range, the data is oversampled before the multi-look filtering is applied. The oversampling is combined with the slant-to-ground range conversion to reduce computational complexity.

9.1.1 Resolution

The natural ground range resolution in the distance unit is approximately

$$\delta_r^o = 1.2 \times 0.89 \times \frac{c}{2B \sin \theta_I},$$

where "0.89" is the factor corresponding to the 3 dB resolution of an ideal sine function and "1.20" represents the resolution broadening caused by the standard processor. The natural azimuth resolution in the distance unit is

$$\delta_a^o = 1.2 \times 0.89 \times \frac{V_{sw}}{PBW}.$$

If δ_r^o and δ_a^o are expressed in the unit of pixels, then

$$\delta_r^o = 1.2 \times 0.89 \times \frac{f_s}{B}$$

$$\delta_a^o = 1.2 \times 0.89 \times \frac{PRF}{PBW}.$$

Let δ_r and δ_a represent the desired resolutions and b, and b_a the associated resolution broadening factors, i.e.,

$$b_r = \frac{\delta_r}{\delta_r^o}$$

$$b_a = \frac{\delta_a}{\delta_a^o}.$$

For SIR-C, the broadening factor varies from 1.0 to 2.5 in range and from 2.5 to 4.0 in azimuth. Recall that for a real digital signal, to recover the signal without any aliasing effect, the sampling rate-to-bandwidth ratio must be greater than or equal to two. For the SIR-C. this sampling rate-to-bandwidth ratio is approximately 1.125 in range and varies from 1.28 to 1.56 in azimuth.

9.1.2 Range Oversampling and Slant-to- Ground Range Conversion

'I'here arc two reasons why the range oversampling and the slant-to-ground range conversion are combined together. The first reason is to reduce additional computational complexity. The second reason is to employ the cubic spline interpolator to interpolate the complex data to preserve the data quality. The weighted sine squared filter will primarily be used to low-pass filter the data to the desired resolution in formation of the multi-look imagery.

The output range pixel spacing is selected to be

$$\Delta r' = \min \left\{ 12.5 \text{ m} \ , \frac{1}{2} 1.2 \times 0.89 \times \frac{c}{2B \sin \theta_I} \right\} .$$

The range resampling indices are generated as follows

$$i + d = \left\{ \frac{\left[R_{et}^2 + (R_{en} + h)^2 - 2R_{et}(R_{en} + h) \cos\left(\frac{R_g + i'\Delta r'}{R_{et}} \right) \right]^{\frac{1}{2}} - r_{sl}}{\frac{c}{2f_s}} \right\} ,$$

where R_g and r_{sl} represent the near range ground range and slant range and i and i' represent the input and output range pixel indices respectively.

$$R_g = R_{et} \cos^{-1} \frac{R_{et}^2 + (h + R_{en})^2 - r_{sl}^2}{2R_{et}(h + R_{en})} .$$

9.1.3 Cross-Products Generation

The next step is to generate the cross-products of the range oversampled, slant-to-ground range converted data, where the cross-products are defined below.

For the quad-polarization data, let the scattering matrix be

$$\mathbf{S} = \begin{pmatrix} S_{HH} & S_{HV} \\ S_{VH} & S_{VV} \end{pmatrix}$$

First of all. average the cross-polarization channel data. Let

$$S_{HV} = \frac{S_{HV} + S_{VH}}{2}.$$

Then, generate six cross-products from the scattering matrix: I_{HHHH}, I_{HHHV}, I_{HVHV}, I_{HHVV}, I_{HVVV} and I_{VVVV}, where

$$I_{HHHH} = S_{HH}S_{HH}^*$$
$$I_{HHHV} = S_{HH}S_{HV}^* \qquad I_{HVHV} = S_{HV}S_{HV}^*$$
$$I_{HHVV} = S_{HH}S_{VV}^* \qquad I_{HVVV} = S_{HV}S_{VV}^* \qquad I_{VVVV} = S_{VV}S_{VV}^*$$

For the single-polarization and the dual-polarization data, the average of cross-polarization data is omitted and only the valid cross-products are generated.

9.1.4 Multi-Look Filter Coefficients Generation

The multi-look filter is required to meet the following requirements:

(a) Be capable to handle variable resolution broadening factors;

(b) Non-negative power;

(c) Small interpolation errors;

(d) Small computational complexity;

(e) Large equivalent number of looks; and

(f) Low sidelobes.

A sufficient condition for the non-negative power requirement is that all the filter coefficients be non-negative. For the SIR-C, the "weighted sine squared filter" is selected, which meets all the above requirements. The procedure to generate the filter coefficients is described below.

(a) Select the desired resolutions;

(b) Compute the initial resolutions;

(c) Compute the resolution broadening factors; and

(d) Use the broadening factor to determine the weighted sine squared filter parameter.

For the SIR-C. the filter length is selected to be 12 points and the number of quantization steps is 32. One filter is generated in range and one in azimuth

Let us use the following notations:

1: filter length;
n: number of bins of the filter;
δ^o: resolution in number of pixels following oversampling;
a: the multi-look filter coefficient used to control the resolution broadening;
N: FFT length used in filter generation; and
N': FFT length used in oversampling.

Also let

$$m = \frac{N}{2\,a\,\delta^o},$$

where $2m$ represents the number of nonzero frequency bins in the spectrum,

The I-point, n-bin weighted sine squared filter coefficients are generated in the frequency domain as follows.

(a) Generate a cosine squared plus pedestal window in the frequency domain.

$$W(i) = \begin{cases} (1-h)\cos^2\left(\frac{\pi i}{2m}\right) + h, & \text{for } 0 \le i \le m-1; \\ 0, & \text{for } m \le i \le N-m-1; \\ (1-h)\cos^2\left(\frac{\pi(i-N)}{2m}\right) + h, & \text{for } N-m \le i \le N-1. \end{cases}$$

where h represents the height of the pedestal function.

(b) Take inverse FFT of W(i) and energy detection, i.e.,

$$w^2(i) = |\mathcal{F}^{-1}(W(i))\ 2\ 0 \le i \le N\ \text{--1},$$

where $w^2(i)$ represents a weighted sine squared function. Notice that the peak occurs at $i = 0$.

(c) Oversample $w^2(i)$ by a factor of n using the FFT oversampling approach, Let the oversampled function be $\hat{w}^2(i)$, where O $\leq i \leq N'$ -- 1 and $N' = n N$.

(d) For an l-point n-bin filter, the filter coefficients are

$$s(j,k) = w^2 \left\{ \left[\left(k - \frac{l}{2} \right) n - j \right] \bmod N' \right\},$$

where O $\leq j \leq n - 1$ and $1 \leq k \leq$ f. To preserve the energy before and after filtering,

$$s(j,k) = \frac{s(j,k)}{\sum_{k=1}^{l} s(j,k)}.$$

The point-target study results show that for the weighted sine squared filter, the multi-look filter parameter, *a*, can be well approximated by a quadratic polynomial function of the resolution broadening factor, *b*, for $1 \leq a < 3$.

$$a = -0.58743 + 1.0448b - 0.035782b^2.$$

This equation is generated assuming that a pedestal height of 0,45 is used in data weighting and a pedestal height of 0.08 is used in filter weighting.

9.1.5 Multi-Look Resampling Indices Generation

Resampling indices show the relationship between the input and output pixel indices. The azimuth resampling indices are generated as follows

$$k + r = \frac{\text{Ax } k'}{V_{sw}} PRF,$$

where ***k*** and ***k'*** represent the input and output azimuth pixel indices respectively.

The range resampling indices are generated as follows

$$i + d = \frac{\Delta r\, i'}{\text{Ar}'}.$$

Note that if Δr = Ar', which occurs for data acquired at steep incidence angles, there is no need for multi-look filtering in range, i.e., the natural resolution will be preserved.

9.2 Data Reduction

9.2,1 Multi-Look Complex Data Reduction

The cross-product data reduction algorithm is selected as the multi-look complex data reduction algorithm for the SIR-C processor.

9.2,1.1 Quad-Polarization Data Reduction

For the quad-polarization data, the data reduction algorithm is as follows. Recall-that the six cross-products are: $I_{HHHH}, I_{HHHV}, I_{HVHV}, I_{HHVV}, I_{HVVV}$ and I_{VVVV}, where

$$I_{HHHH} = S_{HH}S_{HH}^*$$
$$I_{HHHV} = S_{HH}S_{HV}^* \qquad I_{HVHV} = S_{HV}S_{HV}^*$$
$$I_{HHVV} = S_{HH}S_{VV}^* \qquad I_{HVVV} = S_{HV}S_{VV}^* \qquad I_{VVVV} = S_{VV}S_{VV}^*$$

The data reduction is applied to the filtered cross-products as follows.

Let the scale factor be

$$\text{scale} = I_{HHHH} + 2I_{HVHV} + I_{VVVV}.$$

The first output byte is used to represent the exponent of this scale factor

$$\text{Byte(l)} = \text{int}\{\log_2(\text{scale})\}.$$

The second output byte is used to represent the mantissa of this scale factor

$$\text{Byte(2)} = \text{rnd}\{254(\text{MAN} - 1.5)\},$$

where

$$\text{MAN} = \frac{\text{scale}}{2^{\text{Byte(1)}}}$$

Let

$$\text{qsca} = \left(\frac{\text{Byte(2)}}{254} + 1.5\right) 2^{\text{Byte(1)}}.$$

The remaining steps are to normalize all the cross-products by this quantized scale factor. "qsca". Two bytes arc then used to represent each complex cross-product and one byte is

assigned to represent each real cross-product. This results in a total of 10 bytes per output pixel.

$$\text{Byte(3)} = \text{rnd} \quad \overline{\qquad\qquad}$$

$$\{ \quad " \quad ' \quad E \quad \} \quad - \quad] \quad "$$

$$\text{Byte(\$)} = \text{rn}\left\{255\frac{I_{VVVV}}{\text{qsca}}\right\} - 127$$

$$\text{Byte(5)} = \text{rnd}\left\{\text{sgn}[\text{Re}(I_{HHHV})]\ 127\sqrt{\frac{2|\text{Re}(I_{HHHV})|}{\text{qsca}}}\right\}$$

$$\text{Byte(6)} = \text{rnd}\ \underset{\{}{\text{sgn}[\text{Im}(I_{HHHV})]\ 127\sqrt{\frac{2|\text{Im}(I_{HHHV})|}{\text{qsca}}}\Bigg\}}$$

$$\text{Byte(7)} = \text{rnd}\left\{127\frac{\text{Re}(I_{HHVV})}{\text{qsca}}\right\}$$

$$\text{Byte(8)} = \text{rnd}\ \underset{\{}{127\frac{\text{Im}(I_{HHVV})}{\text{qsca}}}$$

$$\text{Byte(9)} = \text{rnd}\ \underset{\{}{\text{sgn}[\text{Re}(I_{HVVV})]\ 127\sqrt{\frac{2|\text{Re}(I_{HVVV})|}{\text{qsca}}}\Bigg\}}$$

$$\text{Byte(10)} = \text{rnd}\ \underset{\{}{\text{sgn}[\text{Im}(I_{HVVV})]\ 127\sqrt{\frac{2|\text{Im}(I_{HVVV})|}{\text{qsca}}}\Bigg\}}.$$

9.2.1.2 Dual-Polarization Data Reduction

For the dual-polarization data, the reduction procedure is similar to that for the quad-polarization data. Let x and y be the polarizations. First of all, generate three cross-products: $I_{xx}(=S_x S_x^*), I_{xy}(=S_x S_y^*)$ and $I_{yy}(=S_y S_y^*)$. These cross-products are filtered to the desired resolution and pixel spacing. The scale factor is the same as that of the quad-polarization except that the cross-products of the non-existing polarizations are set to be zero. Again, two bytes are assigned to the scale factor: one byte to the exponent and the other byte to the mantissa. The other cross-products are then normalized by the quantized scale factor. Two bytes are then used to represent each complex cross-product and one byte is assigned to represent each real cross-product. 'l'he total number of bytes per output pixel is five, The bytes generated are listed as follows.

a) HH and VV polarizations: Byte(l), Byte(2), Byte(4), Byte(7) and Byte(8);

b) HH and HV polarizations: Byte(1), Byte(2), Byte(3), Byte(5) and Byte(6);

c) VH and VV polarizations: Byte(1), Byte(2), Byte(3), Byte(9) and Byte(l O).

9.2.2 Single-Look Complex Data Reduction

The scattering matrix data reduction algorithm is selected as the single-look complex data reduction algorithm for the SIR-C processor. Let us first consider the quad- polarization case. Let the scale factor be

$$\text{scale} = S_{HH}S_{HH}^{*} + S_{HV}S_{HV}^{*} + S_{VH}S_{VH}^{*} + S_{VV}S_{VV}^{*}.$$

The first two bytes are used to represent the exponent and mantissa of the total power.

$$\text{Byte(l)} = \text{int}\{\log_2(\text{scale})\}$$
$$\text{Byte(2)} = \text{rnd}\{254(\text{MAN} - 1.5)\},$$

where

$$\text{MAN} = \frac{\text{scale}}{2^{\text{Byte(1)}}}.$$

Let the quantized scale factor be

$$\text{qsca} = 2\sqrt{\left(\frac{\text{Byte(2)}}{254} + 1.5\right)2^{\text{Byte(1)}}}$$

The scattering matrix data are then coded as follows.

$$\text{Byte(3)} = 127\,\frac{\text{Re}(S_{HH})}{\text{qsca}}$$
$$\text{Byte(4)} = 127\,\frac{\text{Im}(S_{HH})}{\text{qsca}}$$
$$\text{Byte(5)} = 127\,\frac{\text{Re}(S_{HV})}{\text{qsca}}$$
$$\text{Byte(6)} = 127\,\frac{\text{Im}(S_{HV})}{\text{qsca}}$$
$$\text{Byte(7)} = 127\,\frac{\text{Re}(S_{VH})}{\text{qsca}}$$
$$\text{Byte(8)} = 127\,\frac{\text{Im}(S_{VH})}{\text{qsca}}$$
$$\text{Byte(9)} = 127\,\frac{\text{Re}(S_{VV})}{\text{qsca}}$$
$$\text{Byte(1O)} = 127\,\frac{\text{Im}(S_{VV})}{\text{qsca}}$$

The total number of bytes per output pixel is ten.

For both single-polarization and dual-polarization cases, only those available scattering elements are coded. This results in a total of four bytes for the single-polarization data and six bytes for the dual-polarization data.

10. QUALITY ASSURANCE PLAN

Data flow of the SIR-C GDPS Q/A plan is shown in **Fig. 10.1.** These Q/A functions ate employed to assist in understanding the data quality at each processing stage. The proposed Q/A functions (and parameters) consist of several categories:

1. Data Transfer Q/A: performed by the Data Transfer Subsystem during the data transfer:
2. Turn-on and turn-off sequence Q/A: performed by the SAR Correlator Subsystem during the turn-on and turn-off sequence processing;
3. Standard preprocessing Q/A: performed by the SAR Correlator Subsystem during the standard preprocessing;
4. Raw data Q/A: performed by the SAR Correlator Subsystem;
5. Image Q/.4: performed by the SAR Correlator Subsystem;
6. Visual image Q/A: performed by the Output Products Subsystem;
7. Output products Q/A: performed by the Output Products Subsystem;
8. Off-line image Q/A: performed by the Output Products Subsystem; and
9. Calibration Q/A: performed by the Calibration Subsystem.

The first seven Q/A functions are run on a routine basis. The off-line image Q/A function is planned for a more comprehensive analysis of image data in case anomaly effects are observed in the output image data. The calibration Q/A includes parameters such as point-target performance parameters, radiometric and geometric calibration parameters are pre-generated by the Calibration Subsystem.

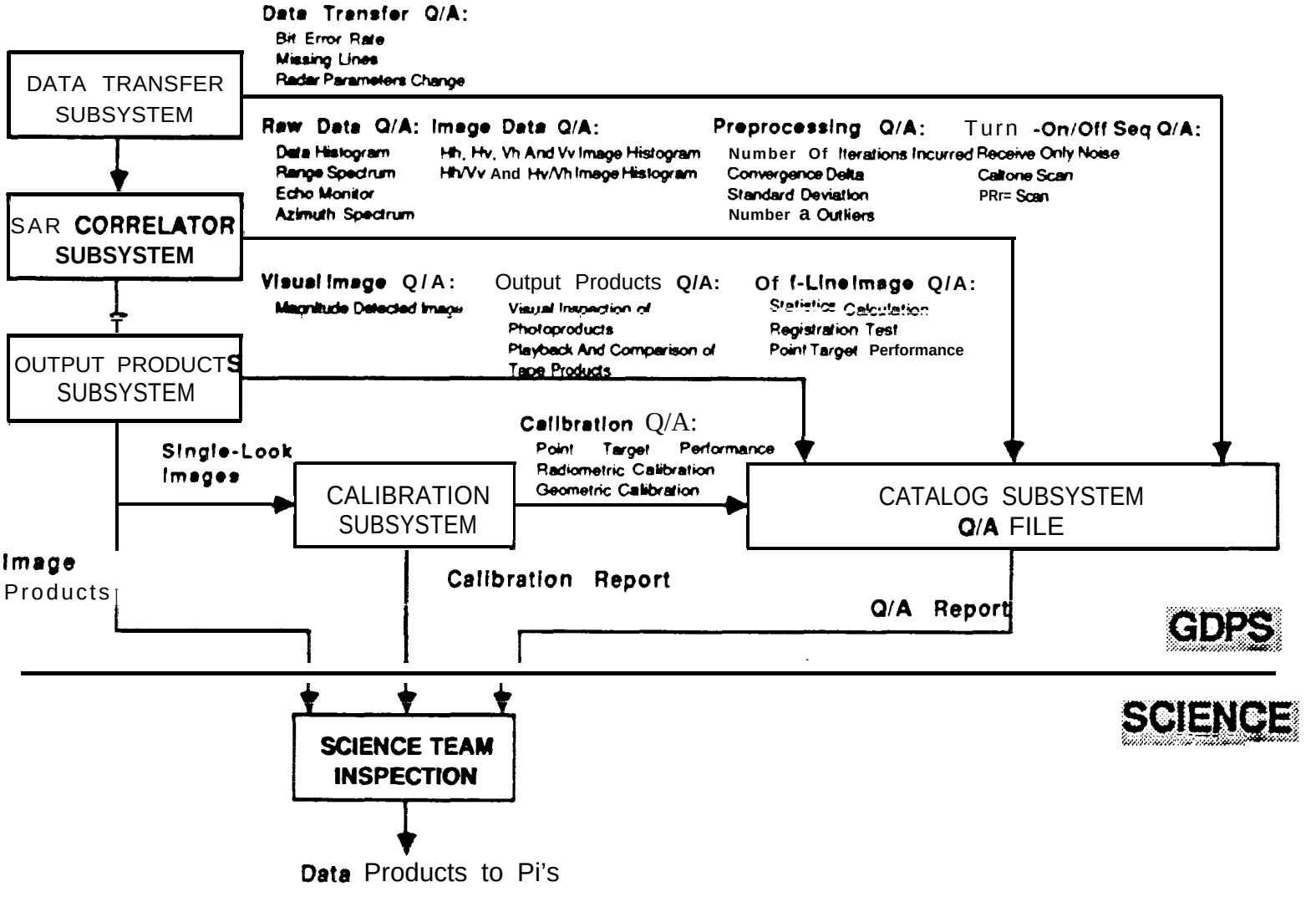

Fig. 10.1: SIR-C Ground Data Processing System data products quality assurance plan.

10.1 Data Transfer Q/A

Data transfer Q/A parameters listed below are derived by the Data Transfer Subsystem during the data transfer.

1. Bit error rate estimate
2. Missing lines
   (a) Total number of missing lines
   (b) Missing lines locations
   (c) Number of flywheels
   (d) Number of locks out of place
   (e) Locations on HDDC
3. Gain change
4. DWP change

10.2 Turn-On and Turn-Off Sequence Q/A

Turn-on and turn-off sequence Q/A parameters listed below are derived by the SAR Correlator Subsystem during the turn-on and turn-off sequence processing.

1. Receive only noise
   (a) Noise power estimate
   (b) Processor noise data gain estimate
2. Caltone scan
   (a) Caltone gain and phase estimates
3. PRF scan
   (a) Ambiguous Doppler centroid estimate
   (b) Unambiguous Doppler centroid estimate
   (c) Doppler centroid delta error
   (d) Number of preprocessing iterations for Doppler centroid frequency
   (e) Allowed number of iterations for Doppler centroid frequency
   (f) Convergence delta for Doppler centroid frequency
   (g) Standard deviation for Doppler centroid frequency

10.3 Standard Preprocessing Q/A

Standard preprocessing Q/A parameters listed below arc derived by the SAR Correlator Subsystem during the standard preprocessing.

1. Preprocessing convergence
   (a) Number of preprocessing iterations for Doppler centroid frequency
   (b) Number of preprocessing iterations for Doppler frequency rate
   (c) Allowed number of iterations for Doppler centroid frequency
   (d) Allowed number of iterations for Doppler frequency rate
   (e) Convergence delta for Doppler centroid frequency
   (f) Convergence delta for Doppler frequency rate
   (g) Standard deviation for Doppler centroid frequency
   (h) Standard deviation for Doppler frequency rate.

10.4 Raw Data Q/A

The raw data Q/A contains five major functions: Range histogram; Range spectrum; Caltone processing; Echo monitor; and Azimuth spectrum. Raw data Q/A parameters listed below are derived at several intervals by the SAR Correlator Subsystem.

1. Range histogram
   (a) Range histogram plot
   (b) Mean
   (c) Standard deviation
   (d) Percent saturation in histogram
2. Range spectrum
   (a) Range spectrum plot
   (b) Signal-to-Noise Ratio estimate
   (c) Range bandwidth estimate
   (d) Spurious peak count in range spectrum
   (e) Spurious peak location in range spectrum
3. Caltone processing
   (a) Caltone gain and phase estimates
   (b) Mean
   (c) Standard deviation
4. Echo monitor
   (a) Echo monitor plot
   (b) Roll angle estimate
5. Azimuth spectrum
   (a) Azimuth spectrum plot
   (b) Azimuth bandwidth estimate.

Fig. **10.2** shows the raw data Q/A algorithm flowchart. The raw data Q/A functions will be performed for each polarization data during the standard processing mode (at start, center and end for a 15-second multi-look processing run; and at start and end for an 8-second single-look processing run), For each interval, 256 range lines are selected to derive the Q/A parameters. During the survey processing mode the raw data Q/A functions are performed at one minute intervals for one polarization channel data. For each interval, the entire processing block data are selected to derive the Q/A parameters. For each range line, the entire range samples are used.

10.4.1 Range Histogram

The range histogram shows the probability of data sample's values (grey levels), from O to 15 for the 4-bit data sample and from O to '255 for the 8-bit and BFPQ data sample. The mean, standard deviation and percentage of saturation arc computed. 'l'he percentage of saturation is defined as the probability of data samples at tails (O and 255 for the 8-bit case). If the percentage of saturation is large, it means that the receiver gain is set too high, which results in clipping of signal. Ideally, the histogram is approximately Gaussian distributed. However, strong ground interference signals may cause the histogram into "bimodal cusp" shape.

For the SIR-C processor, one histogram is generated per polarization per interval during the standard processing mode. Only one histogram is generated per interval during the survey processing mode since only one polarization data is processed.

10,4.2 Range Spectrum

The range spectrum is obtained by incoherently averaging the range spectra (intensity) in the along-track direction, The range spectrum is used to estimate the Signal- to-lNoise Ratio (SNR) and also to detect the interference signals (spikes in the range spectrum). The SNR is computed by taking the ratio of the energy at the center of the spectrum to that at the tails. Interference signals are detected by applying a threshold across the range spectrum.

For the SIR-C processor, one range spectrum is generated per polarization per interval during the standard processing mode. Only one range spectrum is generated per interval during the survey processing mode since only one polarization data is processed.

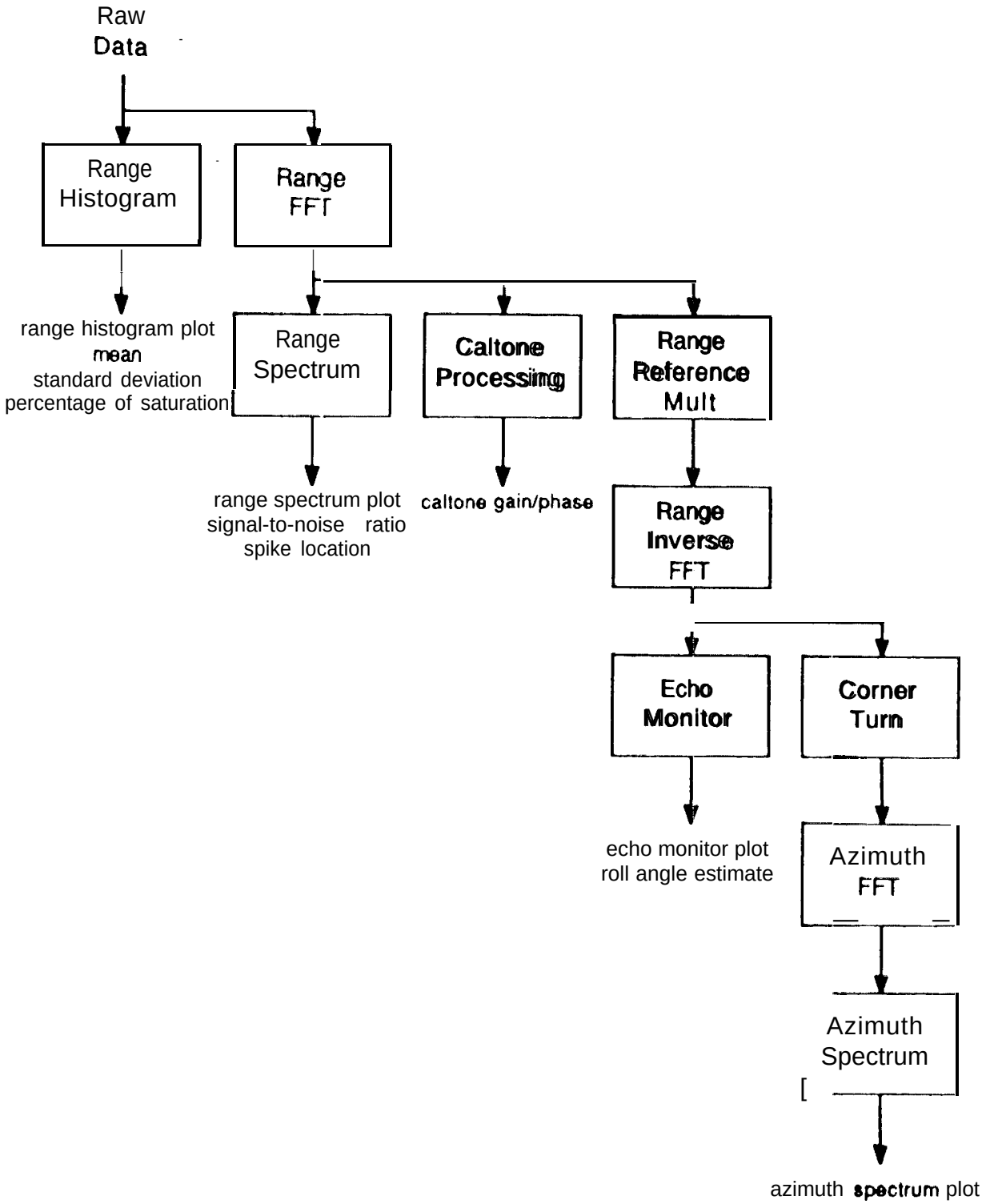

Fig. 10.2: Raw data Q/A algorithm flowchart.

10.4.3 Caltone Processing

The caltone gain is obtained by coherently averaging the range spectra in the along-track direction. The amplitude and phase of the peak of the coherent sum represents the caltone gain and phase, The caltone gain, normalized by a reference caltone gain, is used to characterize the variation in the receiver gain. Because the number of range samples may not be a power of two, a technique known as the caltone signal padding and removal is employed to ensure that the caltone signal will concentrate on the predicted frequency bin in the range spectrum following range FFT.

For the SIR-C' processor, one caltone gain is generated per polarization per interval during the standard processing mode, The three caltone gains generated during the nominal 15 second processing run are checked for short term instability. The three caltone estimates are averaged. The average of the caltone gain estimates is normalized by a pre-selected caltone gain and applied in the range radiometric compensation vector. Only one caltone gain is generated per interval during the survey processing mode since only one polarization data is processed. No averaging is applied.

]0.4.4 Echo Monitor

The echo monitor is obtained by incoherently averaging the range compressed data (intensity) in the along-track direction. The echo monitor is useful to check on the elevation pattern, the correctness of DWP, the existence of nadir return interference.

For the SIR-C processor, one echo monitor is generated per polarization per interval during the standard processing mode. Only one echo monitor is generated per interval during the survey processing mode since only one polarization data is processed.

10.4. s Azimuth Spectrum

The azimuth spectrum is obtained by incoherently averaging the azimuth FFT'ed data in the cross-track direction. The azimuth spectrum is useful to examine the shape of the azimuth antenna pattern.

For the SIR-C processor, one azimuth spectrum (at mid-swath) is generated per polarization per interval during the standard processing mode. Only one azimuth spectrum is generated

per interval during the survey processing mode since only one polarization data is processed. No range migration compensation is applied. Total of 64 azimuth lines are averaged to reduce the noise effect for each azimuth spectrum.

]0.s **Image Q/A**

The image data Q/A parameters (image histogram) are generated by the SAR Correlator Subsystem following the data processing.

1. Image histogram

   (a) Image histogram plot

   (t)) Mean

   (c) Standard deviation

   (d) Percent saturation of histogram

   (e) Image balance

   (f) HV balance

10.6 Visual Image Q/A

Following the completion of each processing run, the output image data will be displayed on the screen on a routine basis. These images will be visually inspected by the operator to detect any noticeable artifacts.

10.7 Output Products Image Q/A

The photoproducts will be visually inspected by the operator to detect any noticeable artifacts.

A subset of the data recorded on the tape will be played back and compared with the reformatted data stored on disk to ensure that the data are correctly written onto tape.

10.8 Off-Line Image Q/A

The off-line image Q/A function is planned for a more comprehensive analysis of image data in case anomaly effects are observed in the output image data. It allows for statistics calculation of the magnitude detected image, the phase difference image and amplitude ratio image of the user selected image block, It also provides functions for point target performance evaluation and multiple channel image registration test.

10.9 Calibration Q/A

"l'he calibration Q/A parameters such as point-target performance parameters, radiometric and geometric calibration parameters are generated by the Calibration Subsystem.

1. Point-target performance
   (a) Nominal slant range resolution
   (b) Nominal azimuth resolution
   (c) 3-dB mainlobe measurement
   (d) 8-dB mainlobe measurement
   (c) Range ISLR
   (f) Azimuth ISLR
   (g) Range PSLR
   (h) Azimuth PSLR
   (i) Range ambiguity
   (j) Azimuth ambiguity
2. Radiometric calibration
   (a) Equivalent number of looks
   (b) Radiometric presentation
   (c) Nominal radiometric resolution
   (cl) Instantaneous dynamic range
   (e) Nominal absolute radiometric calibration magnitude/phase uncertainty
   (f) Nominal relative radiometric calibration magnitude/phase uncertainty
3. Geometric calibration
   (a) Along-track absolute location error
   (b) Cross-track absolute location error
   (c) Along-track scale error
   (d) Cross-track scale error

(e) Along-track relative registration error

(f) Cross-track relative registration error

(g) Skew error

(h) .-A bsolute orientation error,